THE DETERMINATION OF A VOLUMETRIC MIXING LAW FOR USE WITH THE NEUTRON POROSITY LOGGING TOOL

A REPORT SUBMITTED TO THE

STANFORD UNIVERSITY

DEPARTMENT OF PETROLEUM ENGINEERING

IN PARTIAL FULFILLMENT OF THE REQUIREMENTS

FOR THE DEGREE OF

MASTER OF SCIENCE

by

JOSEPH R. SINNER

June, 1986

ABSTRACT

Mixing laws are an instrumental aspect of the interpretation of wireline logs of potential oil and gas wells. Through the use of volumetric mixing laws it is possible to estimate the porosity of a formation from a measure of its density or interval transit time. Estimation of porosity from the neutron logging tool measurements, however, is not based upon a mixing law.

Determination of porosity from a measurement made by a neutron logging tool is currently based on experimental data of similar measurements made in matrices of pure sandstone, pure limestone, or pure dolomite only. The porosities estimated are thus accurate under conditions of pure matrices only; when the matrix consists of a mixture of these three matrix types, slight errors arise. More significant, however, are the errors that arise when shaly sands are encountered. Although the neutron tools actually measure a property of the formation known as the slowing down length, this property has not been used to estimate porosity because no mixing law for it has previously been determined.

This report presents a new mixing law for slowing down length. In addition to its applications in pure matrices, it can be used in matrices containing mixtures of the three principal matrices and anhydrite and also in shaly sands. This is especially useful in shaly sands because of the errors which currently exist when shaly sands are encountered and because of additional applications if the porosity and volume of shale are known from other independent measurements.

ACKNOWLEDGEMENTS

The author wishes to express appreciation to the following: to Darwin Ellis, for the guidance and supervision that made the completion of this research possible; to Schlumberger-Doll Research, for allowing Darwin to come to Stanford and teach logging and for the use of the computer program used to generate the slowing down length **vs.** porosity data; to Stanford University, for financial assistance provided; and to the Stanford Geothermal Program, for financial assistance provided under Department of Energy Contract No. DE-AS03-80SF11459.

CONTENTS

LIST OF FIGURES

Figures 12 through 38 show the comparisons between the slowing down length vs. porosity relationships as generated with the Goertzel-Greuling procedure and as generated using the mixing law detailed in this report. There is one figure for each matrix considered. These matrices are listed below.

1. INTRODUCTION

The interpretation of wireline logs of potential oil and gas wells has been largely dependent upon the development of a variety of mixing laws. There are many well-known mixing laws which relate the volume fractions of the materials encountered and the numerical values of various properties of the materials to numerical values of the properties of mixtures of the materials. Examples of properties for which mixing laws exist include bulk density, interval transit time, and resistivity.

One property commonly measured in wireline logging for which there has previously been no mixing law is the slowing down length, the property measured by most neutron logs. The logging companies currently report the measurements made by their neutron logs in porosity units--that is, the porosity of the formation given that the formation contains a specified matrix. They do this for two reasons: first, because it is porosity which the interpreter ultimately wishes to obtain from the neutron log, and second, because there has been no mixing law with which the interpreter can convert the measured slowing down length to porosity. The central problem with this system is that corrections must be made when the matrix is something other than what has been assumed; additionally, when shaly sands are encountered, the reported porosity of the neutron log reflects more the shale type and content than porosity. A third problem which results from reporting porosity rather than slowing down length is that the corrections which must be made for alternative matrices are dependent upon the specific tool which made the measurement.'

With this in mind, it should be clear that it would be most desirable to have a mixing law for slowing down length; this has been the goal of the research detailed in this report. Before presenting the actual law which was obtained, there is a general discussion of mixing laws currently in use and also a discussion of neutron logging concepts.

2. MIXING LAWS FOR PHYSICAL PROPERTIES

2.1. General Problem

The primary function of a mixing law is to allow an accurate computation of the value of a physical property of a mixture of materials knowing the amounts of each material present and the values of the property for the materials in their pure states. A second function--and the one principally employed in well log analysis--is to allow the computation of the amount of each of the materials present in a mixture given the value of the property for the mixture.

Depending on the specific mixing law, the "amounts" of the materials may mean any of a variety of measured quantities. In some cases, mixing laws are based on the masses of the materials present. In others, the laws use the mole fractions of the materials present. A third type of mixing law is that which is based on the volumes of the materials present. There are others as well. Clearly, the mixing laws which are based on volumes are the most useful laws in analyzing well logs.

Suppose that a mixture of two components has a property g_{mix} and that the individual components of the mixture have properties g_1 and g_2 and volume fractions f_1 and f_2. According to Korvin[2] there are eight physically plausible conditions which, if met, require that the functional form of the relationship between g_{mix}, g_1, g_2, f_1, and f_2 must be

$$g_{mix}^{\alpha} = g_1^{\alpha} f_1 + g_2^{\alpha} f_2 , \tag{2.1.1}$$

where α is some real number or, in the limit as α goes to zero,

$$g_{mix} = g_1^{f_1} g_2^{f_2} . \tag{2.1.2}$$

2.2. Uses In Well Logging

In well log analysis it is usually the case that the two components of interest are a matrix and liquid- or gas-filled pore space; thus, if porosity is denoted by ϕ, Eq. (2.1.1) becomes

$$g_{mix}^{\alpha} = g_1^{\alpha}\phi + g_2^{\alpha}(1-\phi) \tag{2.2.1}$$

and Eq. *(2.1.2)* becomes

$$g_{mix} = g_1^{\phi} g_2^{(1-\phi)} . \tag{2.2.2}$$

There are a number of physical properties of interest in well logging which mix according to ***Eq. (2.2.1).*** Density tool logs report the bulk density of the formation; for bulk density, $\alpha = 1$:

$$\rho_{b_{log}} = \rho_{b_{mat}}(1-\phi) + \rho_{b_f}\phi . \tag{2.2.3}$$

Rearranging the terms leads to the following expression used to determine porosity from a density log:

$$\phi = \frac{\rho_{b_{mat}} - \rho_{b_{log}}}{\rho_{b_{mat}} - \rho_{b_f}} \tag{2.2.4}$$

The density tools actually measure the electron density of the formation and convert it to bulk density. Electron density is proportional to an electron density index ρ_e and the electron density index is related to the bulk density by the following formula:[3]

$$\rho_e = 2\frac{Z}{A}\rho_b , \tag{2.2.5}$$

where Z is the atomic number and *A* the atomic mass. For most materials *Z/A* approx ½ and ρ_e approx ρ_b, but they can differ significantly. The electron density index also mixes with $a = 1$:

$$\rho_{e_{mix}} = \rho_{e_1} f_1 + \rho_{e_2} f_2 + \cdots + \rho_{e_n} f_n . \tag{2.2.6}$$

A third property frequently used in log analysis is the interval transit time *At* associated with the velocity of a compressional sound wave v_c. Wyllie[4] showed that the compressional sound wave velocity *At* mixes with $a = 1$:

$$\Delta t_{log} = \Delta t_{mat}(1-\phi) + \Delta t_f \phi . \tag{2.2.7}$$

Eq. (2.2.7) can be rearranged to obtain an explicit expression for porosity:

$$\phi = \frac{\Delta t_{log} - \Delta t_{mat}}{\Delta t_f - \Delta t_{mat}} \tag{2.2.8}$$

As explained by Hearst and Nelson? the conductivity C and dielectric constant ε at some frequency ω combine as

$$(C_{mix} - i\omega\varepsilon)^{\alpha} = \phi(C_f - i\omega\varepsilon_f)^{\alpha} + (1 - \phi)(C_{mat} - i\omega\varepsilon_{mat})^{\alpha} , \tag{2.2.9}$$

with a typically equal to ½. At low frequencies $\omega\varepsilon$ becomes negligible, and since C_f is much greater than C_{mat} in most rocks, Eq. (2.2.9) reduces to

$$C_{mix}^{\alpha} = \phi C_f^{\alpha} . \tag{2.2.10}$$

Recalling now that conductivity is just the reciprocal of resistivity, i.e,

$$C = \frac{1}{R} , \tag{2.2.11}$$

Eq. (2.2.10) can be restated as

$$\frac{R_f}{R_{mix}} = \phi^{\frac{1}{\alpha}} , \tag{2.2.12}$$

which should be recognized as the expression for Archie's equation at 100% water saturation, with the m of Archie's equation equivalent to $1/\alpha$ in Eq. (2.2.12). If water saturation S_w is less than 100%, the other fluid occupying pore space is also of negligible conductivity compared to the water and so is also ignored. This would lead one to expect that, if water saturation were included in Eq. (2.2.12), the equation would then be

$$\frac{R_w}{R_{mix}} = \phi^{\frac{1}{\alpha}} S_w , \tag{2.2.13}$$

or

$$S_w = \frac{R_w}{\phi^{\frac{1}{\alpha}} R_{mix}} \tag{2.2.14}$$

Interestingly, Archie's equation in its full form is

$$S_w^n = \frac{R_w}{\phi^m R_{mix}} , \tag{2.2.15}$$

with n typically equal to 2. The reason for the appearance of the exponent n is unclear with regard to theoretical mixing law behavior, but it may be that it is included to compensate for the neglected terms.

The final two properties to be discussed with regard to their mixing behavior are the macroscopic neutron cross sections Σ and the macroscopic gamma ray cross section U. The macroscopic neutron cross sections are essentially measures of a material's affinities for various types of interactions with neutrons. They also mix according to Eq. (2.2.1) with $a = 1$:

$$\Sigma_{mix} = \phi\Sigma_f + (1 - \phi)\Sigma_{mat} . \tag{2.2.16}$$

The macroscopic gamma ray cross section, important in lithology logging with gamma rays, is the product of the photoelectric index P_e and the electron density index ρ_e:[6]

$$U = P_e\rho_e . \tag{2.2.17}$$

There are logging tools which measure the photoelectric index, but it is the macroscopic gamma ray cross section U for which Eq. (2.2.1) applies--again with $a = 1$:

$$U_{mix} = \phi U_f + (1 - \phi)U_{mat} . \tag{2.2.18}$$

Since the electron density index ρ_e also mixes with $a = 1$, the manipulation of Eq. (2.2.18) to get the photoelectric index P_e can be done quite easily.

3. CONCEPTS OF NEUTRON LOGGING

The material presented in this section comes primarily from the following sources: papers by Tittle? Tittle and Allen,[8] and Allen et al[9] and books by Ellis[10] and Hearst and Nelson.[11]

3.1. Neutron Emission

The most common neutron sources currently used by the logging companies are chemical sources consisting of Be and either Pu or Am. Both Pu and Am emit alpha particles; the alpha particle combines with the Be to produce a neutron and either three more alpha particles or a ^{12}C nucleus. These reactions may be written as

$$^{9}Be + {}^{4}He \rightarrow 3\,{}^{4}He + n + Energy \qquad (3.1.1)$$

and

$$^{9}Be + {}^{4}He \rightarrow {}^{12}C + n + Energy\ . \qquad (3.1.2)$$

Additional alternatives to Pu and Am include Ra and Po; similarly, B and Li can be used instead of Be. The neutrons produced by these reactions have energies ranging from about 0.1 to 10 MeV; as shown in Fig. 1, the *peak* of the energy spectrum occurs at about 4 MeV. Figure 1 also shows the classification scheme for neutron energies. The boundaries of the energy ranges are quite arbitrary and some scientists include an intermediate region, but the scheme is useful nevertheless.

Another source of neutrons currently used in well logging applications is the combination of hydrogen isotopes ^{2}H (deuterium) and ^{3}H (tritium), producing an alpha particle and a neutron:

$$^{2}H + {}^{3}H \rightarrow {}^{4}He + n + Energy\ . \qquad (3.1.3)$$

Neutrons produced by this mechanism have energies of about 14 MeV (Fig. 1). This mechanism has both advantages and disadvantages over the chemical sources: it involves a particle accelerator which *can* be turned on and off and so is much safer than the chemical sources. and

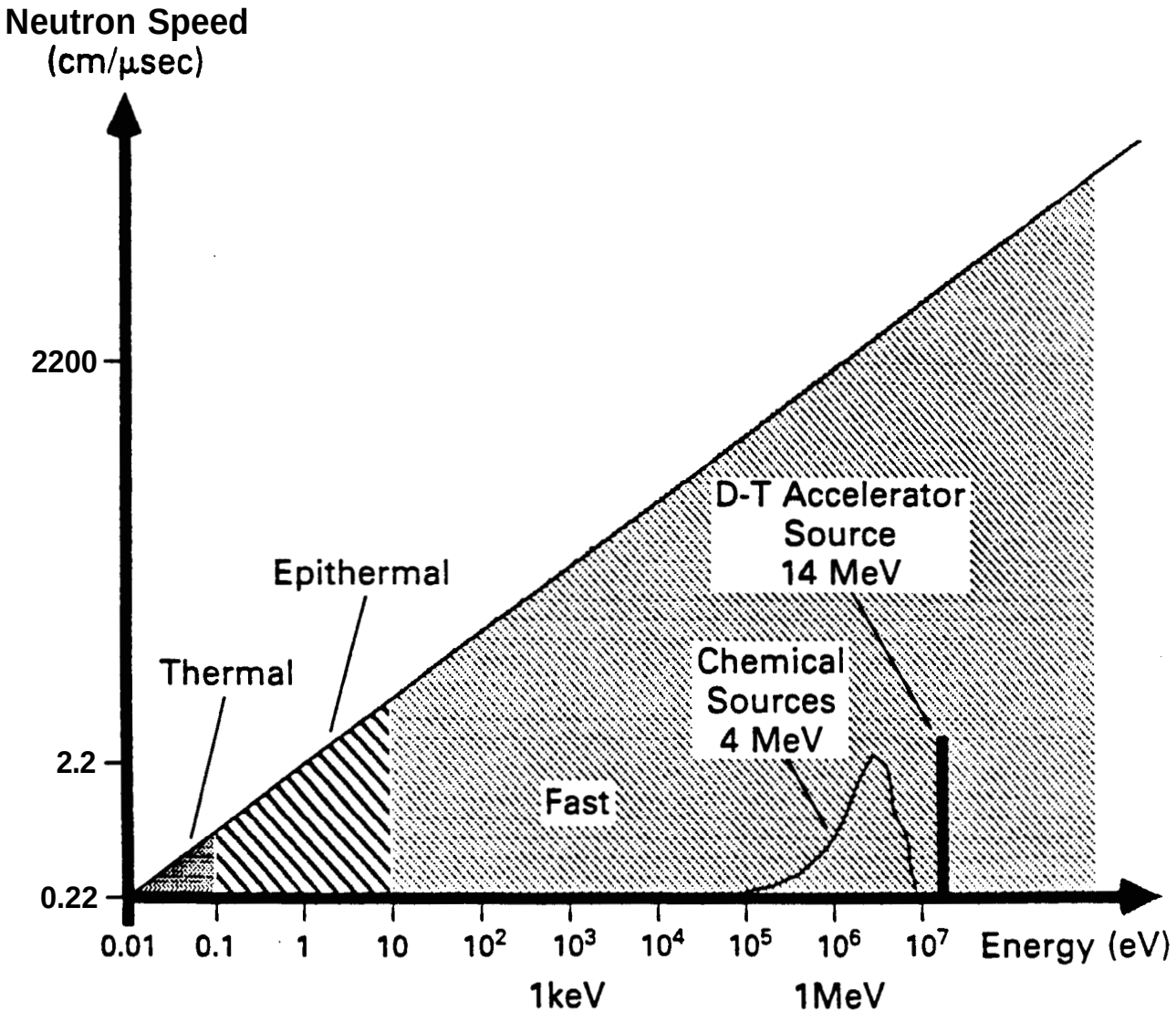

Figure 1. The relationship between neutron energy and speed for the three broad classifications of neutron energies. [From Ellis, Ref. 10.]

the high energy neutrons produced give rise to some interesting reactions in the formation which the lower energy neutrons do not, but it is also much more expensive and less reliable than the use of chemical sources.

3.2. Neutron-formation Interaction

As the neutrons leave the source within the logging tool and enter the formation they collide with many nuclei, losing energy and slowing down with time. There are four principal types of interactions: fast reactions, inelastic scattering, elastic scattering, and radiative capture; the one most likely to occur in a given collision depends largely upon the energy of the neutron.

Fast reactions and inelastic scattering occur more frequently at high energies. Both involve the neutron combining with a nucleus to create a compound nucleus in an excited, unstable state. In the case of inelastic scattering, the compound nucleus quickly decays, releasing a gamma ray and then a neutron, thus returning to the atomic configuration it had before the collision with the neutron. In fast reactions, which have a small probability of occurrence, the compound nucleus emits any of a variety of charged particles instead of a neutron, and so does not return to the atomic configuration it had before the collision. Due to their small probability of occurrence, neither of these two types of interactions has a significant impact in slowing down the overall population of neutrons.

Elastic scattering occurs over the entire energy range of interest. In this type of interaction a neutron simply collides with a nucleus and bounces away, transferring some, none, or all of its energy of motion to the nucleus. The amount of energy a neutron loses in such a collision depends upon both the mass of the nucleus and the "directness" of the collision. By analysis of the principles of conservation of energy and momentum it can be shown that the ratio between the neutron's energy after the collision E and the neutron's energy before the collision E_o is

$$\frac{E}{E_o} = \frac{A^2 + 2A\cos\theta + 1}{(A+1)^2}, \qquad (3.2.1)$$

where A is the atomic mass of the nucleus and θ is the angle between the line of departure of the neutron and the line of travel the neutron would have taken had it not collided with the nucleus. Maximum energy loss occurs in a direct collision; i.e., when the neutron bounces directly back in the direction from which it came. In this case $\theta = 180°$ and Eq. (3.2.1) reduces to

$$\frac{E}{E_o} = \frac{(A-1)^2}{(A+1)^2} . \qquad (3.2.2)$$

From Eq. (3.2.2) it can be seen that as A increases, the ratio approaches unity and the energy loss is minimal. If $A = 1$ (hydrogen), however, a direct collision will result in a complete loss of the neutron's energy. Elastic collisions—especially with hydrogen nuclei--are the primary mechanism by which the neutron population slows down and are also the key to understanding the use of the neutron logs for determining porosity. By measuring the formation's ability to slow down the neutrons, the neutron tools are essentially responding to the formation's hydrogen content, and hydrogen exists almost exclusively in pore fluids such as oil and water.

Radiative capture, the fourth principal type of interaction, occurs only at low neutron energies. Because of its low energy, the neutron is absorbed by the target nucleus and disappears. This also results in the emission of a gamma ray.

The probability of a given interaction taking place with a single nucleus is referred to as a cross section, denoted by σ and measured in square centimeters or barns. One barn equals 10^{-24} cm^2. There is a cross section for each type of interaction: $\sigma(n,n)$ for elastic collisions, $\sigma(n,n')$ for inelastic collisions, $\sigma(n,x)$ for reactions, and $\sigma(n,\gamma)$ for radiative capture. The sum of the individual interaction σ's is called the total cross section and is denoted by σ_{tot}. Figure 2 shows how the cross sections discussed above vary with the energy of the neutron.

When dealing with material on a larger scale, the cross sections are expressed differently. The macroscopic cross section for an interaction of type i is denoted by Σ_i and is defined as the product of the cross section for that interaction σ_i and the number of atoms per cubic centimeter:

$$\Sigma_i = \frac{N_A \rho_b}{A} \sigma_i , \qquad (3.2.3)$$

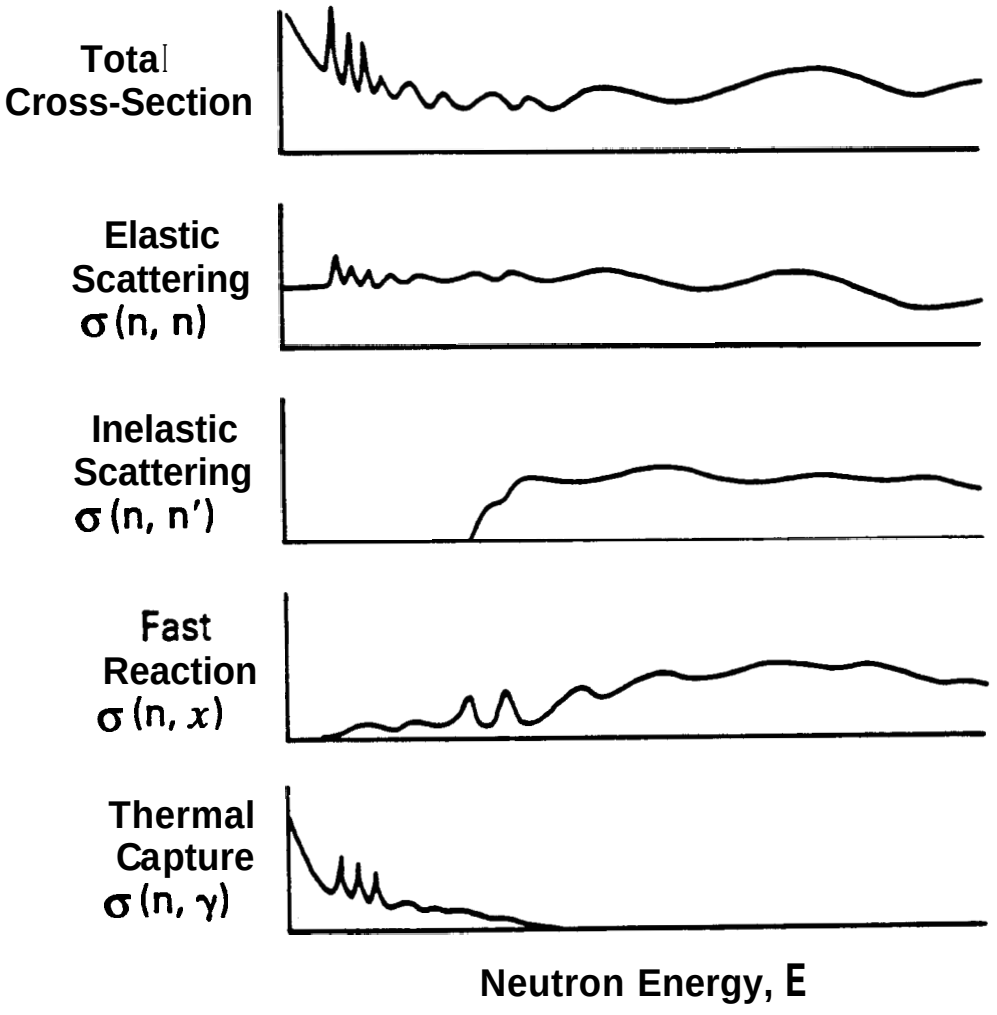

Figure 2. A schematic illustration of the components involved for the total cross section as a function of energy. The characteristics of four specific cross sections are shown. (After Ellis, Ref. 10.)

where N_A is Avagadro's Number (6.022×10^{23} atoms per mole), A is the atomic mass in grams per mole, and ρ_b is the bulk density in grams per cubic centimeter. Since σ has units of cm^2, the units of Σ must be cm^{-1}. The reciprocal of Σ is defined as the mean free path λ that a neutron travels between interactions of type i.

As mentioned previously, the interactions between the neutrons and the nuclei of the formation cause an energy loss in the overall neutron population. In addition to Σ there are three other parameters useful for describing the formation's interaction with bombarding neutrons. These parameters are the slowing down length L_s, the diffusion length L_d, and the migration length L_m. All are measured in length units, typically centimeters.

The slowing down length is a measure of the average distance neutrons travel in a medium in slowing down from a specific initial energy to a specific final energy. In addition to being dependent upon the initial and final energy states, the slowing down length is also a function of the scattering cross sections of the materials in the medium and the average energy lost per interaction. Kreft[12] detailed a method by which the slowing down length of a medium can be calculated. As will be discussed shortly, it is this property that is measured in some neutron porosity devices.

As stated earlier, most logging devices currently use chemical sources which generate neutrons having energies of about 4.2 MeV on average. The epithermal detectors currently used detect neutrons having energies of around 1.5 eV. Defining these energy levels as the initial and final energy states, the slowing down length of various materials were calculated. Table 1 lists the slowing down length of some pure substances and Fig. 3 shows how slowing down length varies with porosity for sandstone, limestone, and dolomite.

The diffusion length is a measure of how far a neutron travels between the point at which it became a thermal neutron and the point at which it is absorbed by a nucleus. It can be calculated with knowledge of the thermal diffusion coefficient D_{th} and macroscopic thermal absorption cross section Σ of the material by the following formula:

$$L_d = \sqrt{\frac{D_{th}}{\Sigma}} . \qquad (3.2.4)$$

Table 1. Slowing Down Lengths† of Pure Substances	
Material	L_s, cm
Water	7.67
Sandstone	28.79
Limestone	25.69
Dolomite	21.28
Anhydrite	31.38
Illite	14.54
Kaolinite	9.07

† from 4.2 MeV to 1.5 eV

Calculation of the diffusion coefficient D_{th} also requires knowledge of the cross sections of the material.

The migration length is used primarily for convenience in thermal neutron porosity devices and is defined as follows:

$$L_m = \sqrt{L_s^2 + L_d^2} \,. \tag{3.2.5}$$

33. Neutron Detection

The detection of neutrons is accomplished through the use of a target material which, after absorbing a neutron, produces a charged particle. The charged particle causes ionization which can be measured by a device such as a proportional counter. For any such target material, its ability to absorb a neutron will vary with the energy of the neutron, and since it is the detection of thermal and epithennal neutrons which is currently of most use in well logging, the target material will ideally absorb very efficiently at low neutron energies and very inefficiently at energies above that which is desired for detection.

For the detection of thermal and epithermal neutrons, there are three principal target nuclei in use: '%, %, and ^{3}He, the most common of which is ^{3}He. Both ^{10}B and ^{6}Li emit an alpha particle following the absorption of a neutron, while ^{3}He emits a proton.

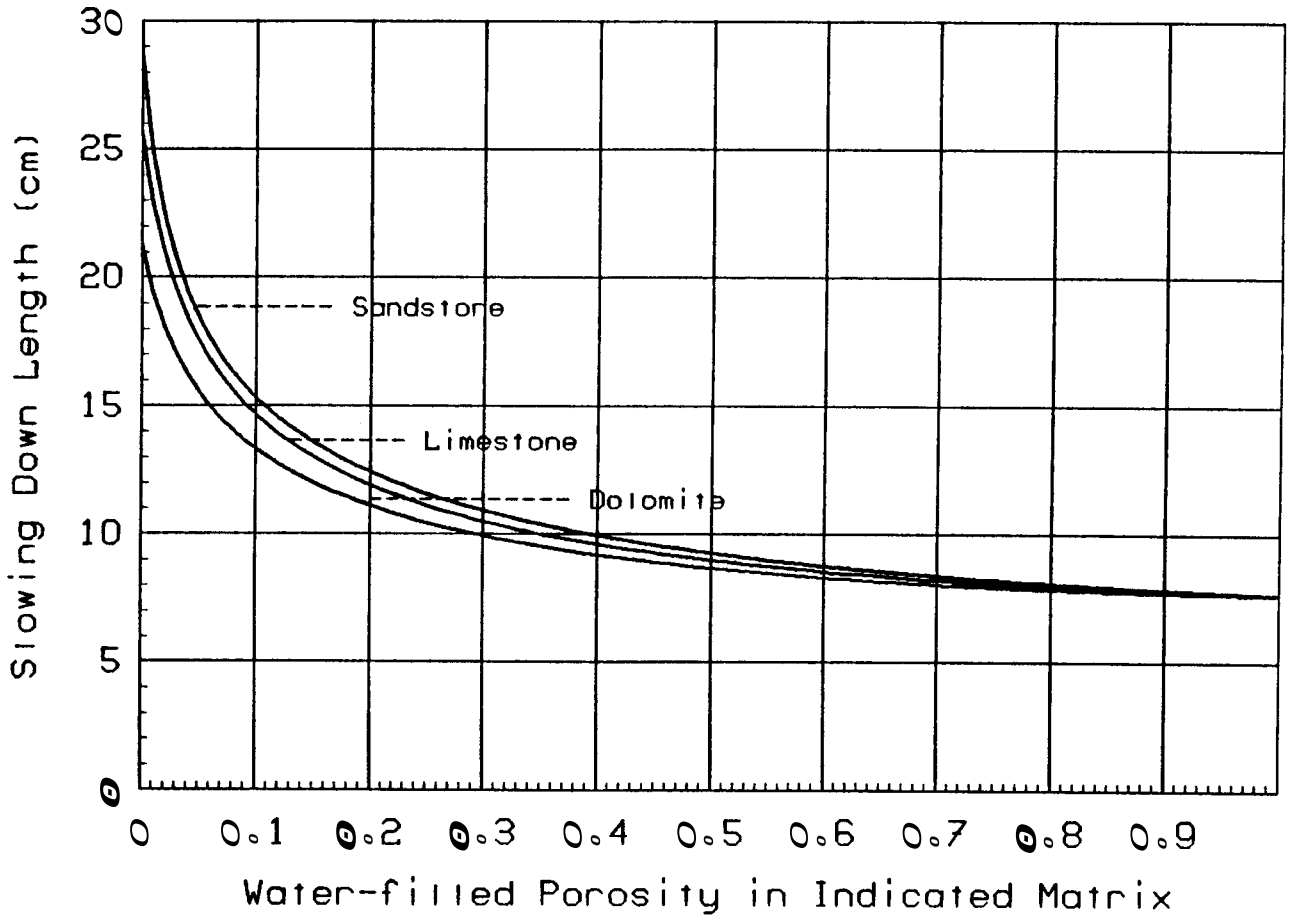

Figure 3. Slowing down length vs. water-filled porosity in sandstone, limestone, and dolomite. Initial energy is 4.2 MeV and final energy is 1.5 eV.

If one desires to detect only epithermal neutrons, as is the case in some logging applications, the target material can be surrounded by an efficient thermal neutron absorber which allows transmission of the slightly higher energy epithermal neutrons. The material currently used the most for this purpose is cadmium.

3.4. Current Interpretation Techniques

Allen et al[9] showed that the epithermal neutron count rate Φ_{ep} of a detector at a distance r from a neutron point source of strength Q is given by the equation

$$\Phi_{ep}(r) = \frac{Q}{4\pi D_{ep}} \frac{e^{\frac{-r}{L_s}}}{r}, \tag{3.4.1}$$

where D_{ep} is the epithermal diffusion coefficient and L_s is the slowing down length. They also showed that for source-detector spacings of 70 centimeters or greater, the thermal neutron count rate Φ_{th} can be reasonably approximated by

$$\Phi_{th}(r) \approx \frac{QL_d^2}{4\pi D_{th}(L_s^2 - L_d^2)} \frac{e^{\frac{-r}{L_s}}}{r} \tag{3.4.2}$$

In both cases, if one takes the ratio of count rates measured at two detectors at distances r_1 and r_2, all terms except the distances and the slowing down length cancel. For epithermal neutrons, the ratio is exact:

$$\frac{\Phi_{ep}(r_2)}{\Phi_{ep}(r_1)} = \frac{r_1}{r_2} e^{\frac{1}{LS}(r_1 - r_2)}. \tag{3.4.3}$$

For thermal neutrons, the ratio is a very reasonable approximation if both detectors are at least 70 centimeters from the source:

$$\frac{\Phi_{th}(r_2)}{\Phi_{th}(r_1)} \approx \frac{r_1}{r_2} e^{\frac{1}{LS}(r_1 - r_2)}. \tag{3.4.4}$$

Solving for the slowing down length L_s gives

$$L_s = \frac{r_1 - r_2}{\ln\left[\frac{r_2}{r_1}\frac{\Phi(r_2)}{\Phi(r_1)}\right]}, \qquad (3.4.5)$$

where Φ can be either the epithermal or thermal neutron count rate. Figure 4 shows a typical relationship between the ratio of the detection rates and slowing down length.

Currently, logging companies assume a matrix and, using the ratio of the count rates of two detectors, determine porosity from a data set of porosity vs. detection ratios for the assumed matrix. In other words, they essentially bypass Eq. (3.4.5). Although these data sets and Fig. 3 are for water-filled porosity, they work equally well for porosity containing liquid hydrocarbons since water and liquid hydrocarbons have approximately the same effect on the formation's overall slowing down length. If the formation contains gas, if the matrix contains shale, or if the matrix is different from the one assumed, errors arise.

Because gas at reservoir conditions can be of much lower density than either oil or water, it does not have nearly the impact on lowering the formation slowing down length that the liquids do. Consequently, the derived porosity appears to be lower. This gives rise to the well-known gas effect; indeed, the neutron log is frequently employed for the sole purpose of gas detection because of the cross-over that occurs between the neutron and density porosity logs in gas sands. The cross-over occurs because, along with the neutron log reporting a value too low, the density-derived porosity is too high, since it also is correlated on liquid-filled porosity. When it measures low density, it reports high porosity. When gas is encountered, the algorithm converts the extremely low density to extremely high porosity.

Shales, like water and oil, have low slowing down length values. Their presence thus lowers the measured slowing down length, which in turn causes the porosity to appear higher than it actually is. This is shown graphically in Fig. 5 for two shaly sands, one containing 25% illite and one containing 25% kaolinite. As Fig. 5 shows, if the matrix is a shaly sand containing 25% kaolinite and the porosity is 10%, then the slowing down length is about 12.5 centimeters. If this shale is not considered and the matrix is assumed clean (as is currently

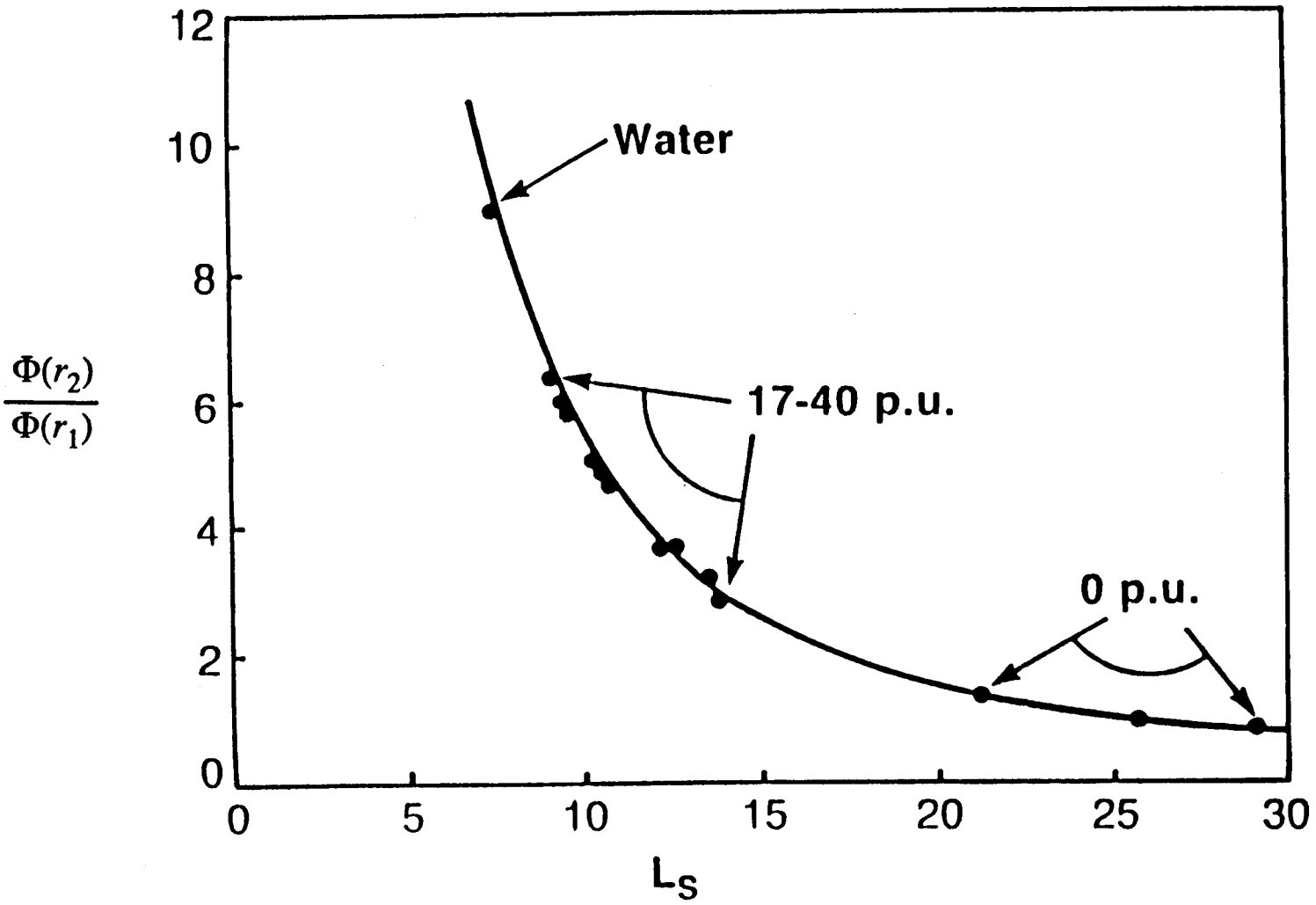

Figure 4. Response of an experimental epithermal device as a function of slowing down length in cm. Data includes points for sandstones, limestones, and dolomites. $r_1 > r_2$. (From Ellis, Ref. 13.)

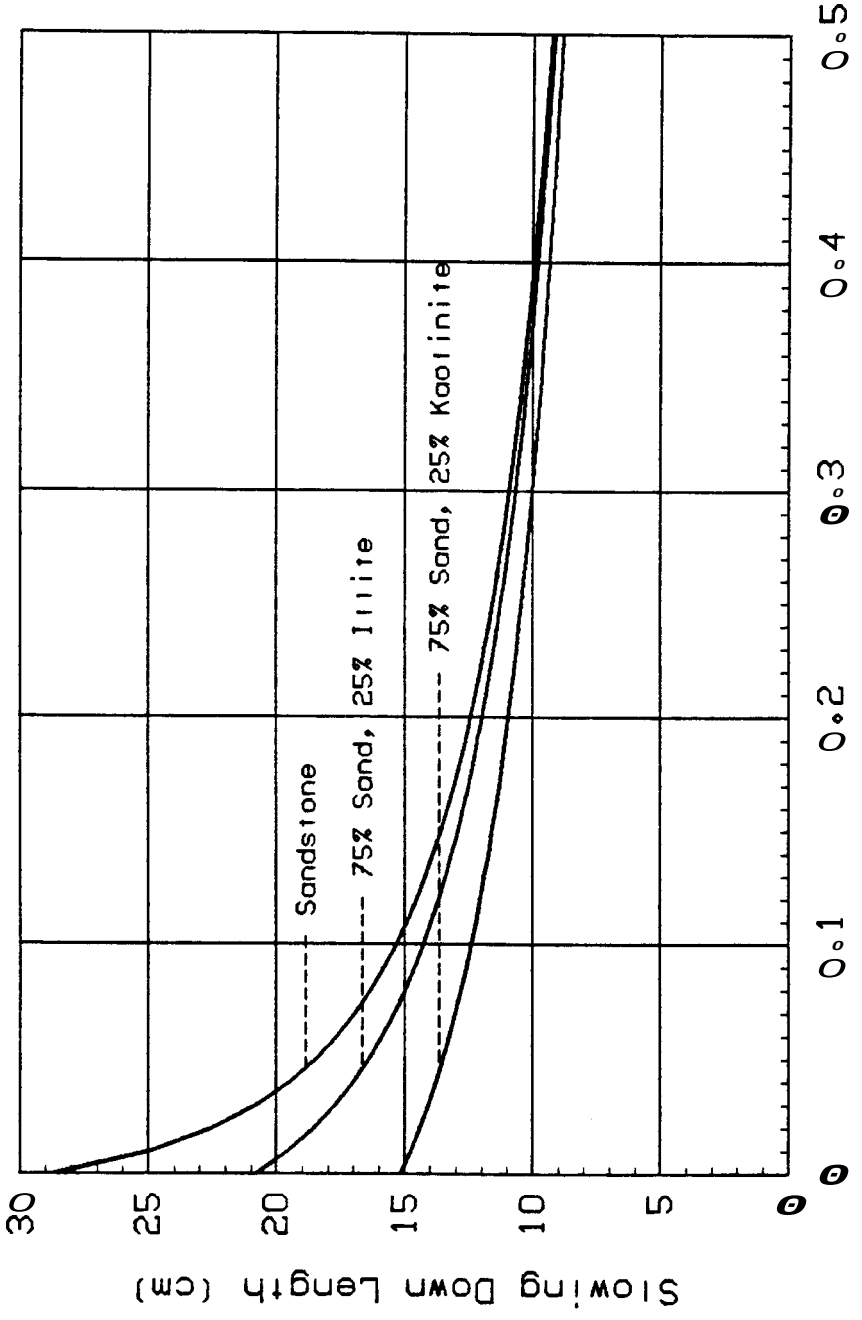

Figure 5. Slowing down length vs. water-filled porosity in pure sandstone and two shaly sands. Initial energy is 4.2 MeV and final energy is 1.5 eV.

done when processing log data to report neutron porosity), porosity would be estimated at about 21%, more than twice its actual value. Similarly, a 10% porosity shaly sand whose matrix contains 25% illite has a slowing down length of about 14.3 centimeters; if assumed clean, porosity would be estimated at about 13%. Though high readings such as these may be useful for indicating shaly sands, they obviously reduce the usefulness of the reported porosity. It would perhaps be more useful if a log interpreter had knowledge of the slowing down length itself for attempting to determine an accurate value of porosity.

When using the standard porosity output, if a matrix other than the one assumed is encountered, the log interpreter must refer to a correction chart given in the log interpretation chart books provided by the logging companies. The need for correction can be seen in Fig. 3. If slowing down length were reported, the interpreter would not have to make corrections. However, charts or equations would still be required, but the interpreter would be less likely to work with an incorrect mamx since he would have to assign it in each case.

4. A MIXING LAW FOR SLOWING DOWN LENGTH

4.1. Determination of the Mixing Law

In order to determine a mixing law for slowing down length it was necessary to first generate data sets of slowing down length vs. porosity for a variety of 14 different combinations of the principal matrices and 13 shaly sands, similar to those for sandstone, limestone, and dolomite plotted in Fig. 3. Because porosities encountered in logging rarely exceed 50%, it was decided that these data sets should cover only the range of 0 to 50% porosity, with values of slowing down length calculated at 1% intervals. The justification for this is that any mixing law subsequently derived would be based on the points of interest; i.e., it would not be weighted by points involving unrealistic porosities. Edmundson and Raymer[14] point out that accurate values for slowing down length *can* probably be calculated only by using time-consuming and costly Monte Carlo methods or numerical solutions to the Boltzman transport equation, but that reasonable approximations are possible using a method called the Goertzel-Greuling procedure. The Goertzel-Greuling procedure was used to generate the data* for the curves for this analysis. A description of the procedure can be found in Reference 15. All slowing down length calculations were based on an initial neutron energy of 4.2 MeV and a final energy of 1.5 eV.

The next step was to try various forms of mixing laws and determine both the optimal values of any numerical constants involved in the law and the errors which resulted from its use. This was done using a FORTRAN program which exploited the IMSL subroutine ZXSSQ.[16] Subroutine ZXSSQ performs a non-linear, least squares analysis of a function and determines for a particular data set the best values for any constants in the function. The form of the initial equation tried was that of Eq. (2.2.1); i.e.,

$$L^{\alpha}_{s,mix} = L^{\alpha}_{s,w}\phi + L^{\alpha}_{s,mat}(1-\phi) \tag{4.1.1}$$

*An operational Goertzel-Greuling program was obtained from Schlumberger-Doll Research, Ridgefield, Connecticut.

The optimal value of a varied greatly from matrix to matrix, and the resulting errors were quite large, indicating that the slowing down length does not meet the requirements for this type of law as outlined by Korvin.[2] Because a power law did show some promise, however, it was decided that a slight modification of Eq. (4.1.1), that of adding a constant k to L_s before raising it to the power a, should be tried. This can be mathematically stated as:

$$(L_{s,mix} + k)^{\alpha} = (L_{s,w} + k)^{\alpha}\phi + (L_{s,mat} + k)^{\alpha}(1 - \phi) . \qquad (4.1.2)$$

This form presented excellent results, with virtually no error. There was still significant variance in the values of a, but the values of k were mostly in the range of about -4 to -5. It was then postulated that setting the value of k to a specific value might cause the value of a to change enough to compensate for the errors in the cases for which k was furthest from the specific value chosen. For simplicity the value of k was set at -4.5, resulting in the following form of the equation:

$$(L_{s,mix} - 4.5)^{\alpha} = (L_{s,w} - 4.5)^{\alpha}\phi + (L_{s,mat} - 4.5)^{\alpha}(1 - \phi) . \qquad (4.1.3)$$

Though some small errors resulted, particularly in pure dolomite, the results were quite good. Furthermore, two interesting relationships were noticed for the values of a. First, for matrices which contained no shale, the value of a appeared to depend on $L_{s,mat}$, the slowing down length of the matrix. Second, for shaly sands containing up to 25% shale, the value of a did not vary significantly from the value of a for pure sandstone. Table 2 gives the values of $L_{s,mat}$ and a for the matrices containing no shale and Table 3 gives the same data for shaly sands.

The data in Tables 2 and 3 are plotted in Fig. 6, clearly showing the relationship between a and $L_{s,mat}$ for the matrices containing no shale. In order for Eq. (4.1.3) to be useful, however, one must be able to determine both a and $L_{s,mat}$. If these two parameters are known, one can compute porosity ϕ from a measured formation slowing down length $L_{s,mix}$, or $L_{s,log}$. By close examination of the data in Tables 2 and 3 and Fig. 6, it was noticed that, for the "clean" matrices, the fitting power a is very close to a volume fraction-weighted sum of the fitting powers

Table 2. Slowing Down Lengths and Fitting Powers for Matrices Containing No Shale

Matrix Number	Matrix	$L_{s,mat}(cm)$	α
1	Sandstone	28.79	-1.664
2	Limestone	25.69	-1.745
3	Dolomite	21.28	-2.001
4	Anhydrite	31.38	-1.653
5	50% Sand, 50% Lime	26.83	-1.706
6	75% Lime, 25% Dol	24.39	-1.803
7	50% Lime, 50% Dol	23.24	-1.865
8	25% Lime, 75% Dol	22.21	-1.930
9	90% Lime, 10% Anhy	26.13	-1.735
10	80% Lime, 20% Anhy	26.59	-1.726
11	90% Dol, 10% Anhy	21.95	-1.958
12	80% Dol, 20% Anhy	22.67	-1.918
13	45% Lim, 45% Dol, 10% An	23.82	-1.840
14	40% Lim, 40% Dol, 20% An	24.45	-1.816

Table 3. Slowing Down Lengths and Fitting Powers for Shaly Sands

Mamx Number	Matrix	$L_{s,mat}(cm)$	a
15	95% Sand, 5% Illite	26.24	-1.641
16	90% Sand, 10% Illite	24.38	-1.623
17	85% Sand, 15% Illite	22.94	-1.609
18	80% Sand, 20% Illite	21.78	-1.596
19	75% Sand, 25% Illite	20.82	-1.586
20	95% Sand, 5% Kaolinite	22.61	-1.621
21	90% Sand, 10% Kaolinite	19.56	-1.612
22	85% Sand, 15% Kaolinite	17.62	-1.622
23	80% Sand, 20% Kaolinite	16.23	-1.646
24	75% Sand, 25% Kaolinite	15.16	-1.682
25	90% Sand, 5% Ill, 5% Kao	21.50	-1.610
26	80% Sand, 10% Ill, 10% Kao	18.31	-1.603
27	70% Sand, 15% Ill, 15% Kao	16.37	-1.620

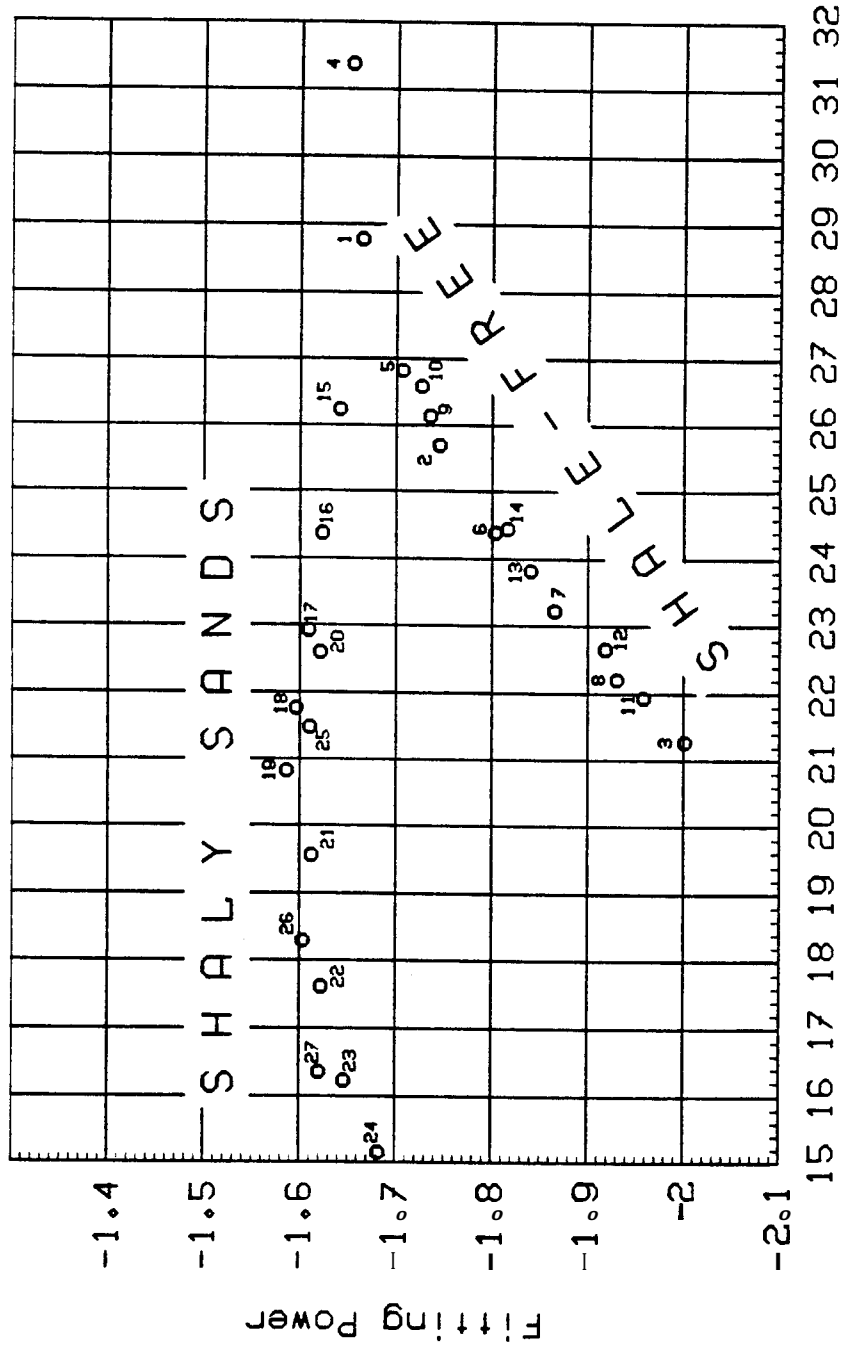

Figure 6. Fitting power vs. slowing down length of matrix. Numbers refer to matrices as indicated in Tables 2 and 3.

of the components. That is,

$$a = \sum_{i=1}^{n} \alpha_i f_i \ , \qquad (4.1.4)$$

where n is the number of different matrices in the matrix mixture and f_i is the volume fraction of matrix i. Thus, for example, if the matrix encountered is 25% limestone and 75% dolomite, the fitting power is one-fourth the fitting power of limestone plus three-fourths the fitting power of dolomite. A best fit of a quadratic equation was then found to determine an equation which would yield L_{ss} given a for the non-shaly matrices. The relationship found, shown graphically in Fig. 7, is as follows:

$$L_{ss} = 37.83\alpha^2 + 159.3\alpha + 188.75 \ . \qquad (4.1.5)$$

In obtaining Eq. (4.1.5), the pure anhydrite point was not included because it deviates somewhat from the relationship and because matrices containing greater than about 20% anhydrite are relatively rare. Thus, no points for matrix mixtures will lie near the anhydrite point.

For shaly sands, Fig. 6 shows that the fitting powers all lie in the range of about -1.59 to -1.68. Using a value somewhere in the middle of this range, e.g., -1.63, yields the best results in predicting $L_{s,mix}$ from porosity, but even the pure sandstone fitting power of -1.664 is sufficient. The determination of $L_{s,mat}$, however, is more difficult. Because the presence of shale affects the slowing down length in the same way that the presence of water does, it is possible to correlate the amount of shale present in the matrix to an equivalent clean sandstone porosity ϕ_{ss}. ϕ_{ss} is the porosity that a clean sand would have if it had a slowing down length equal to the *matrix* slowing down length of the shaly sand. Only two shales--illite and kaolinite--were considered because all shales contain either $(OH)_4$ or $(OH)_8$ groups and it is the presence of these hydroxyls which causes the reduction in the slowing down length. Illite contains $(OH)_4$ groups and kaolinite contains $(OH)_8$ groups; thus, kaolinite is more effective in lowering the matrix slowing down length. The relationships between ϕ_{ss} and the shale volume fractions are depicted in Fig. 8. It is important to note that the shale fractions act independent-

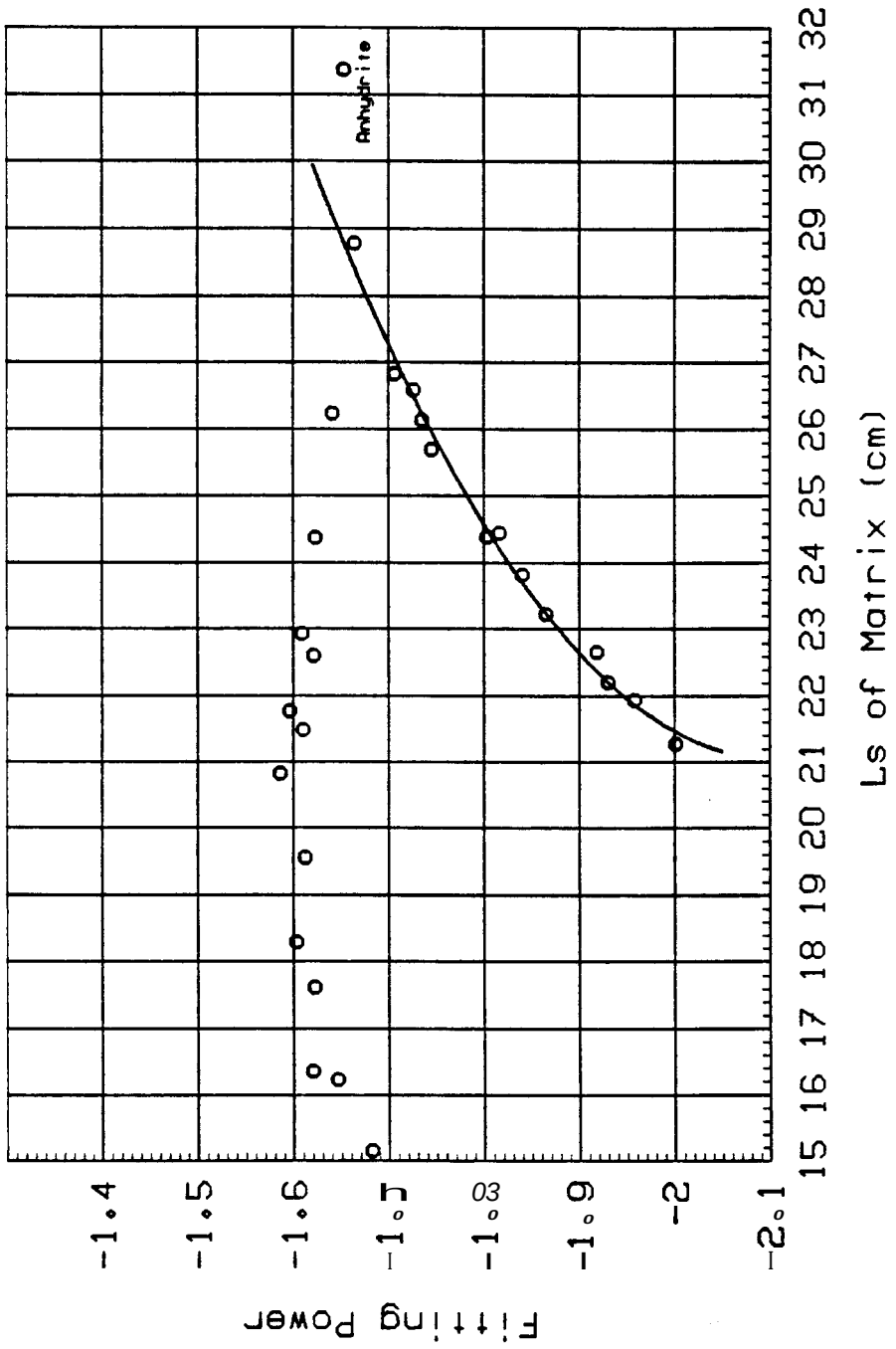

Figure 7. Fitting power vs. slowing down length of matrix. This figure shows the graphical form of Eq. (4.1.5).

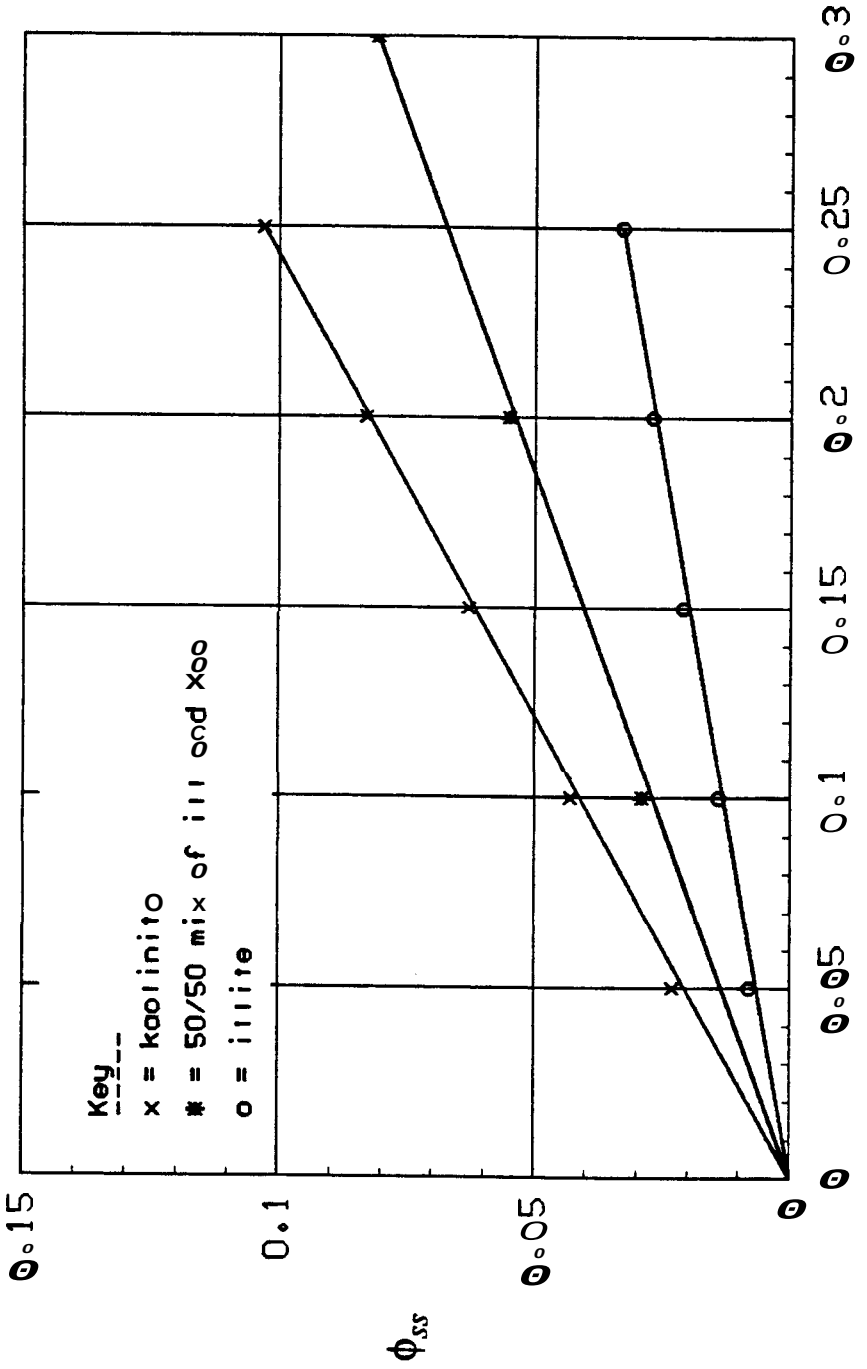

Figure 8. Equivalent clean sandstone porosity vs. volume fraction of shale in the matrix for three different shale types.

ly in reducing the matrix slowing down length. As shown in Fig. 8, the equivalent clean sandstone porosity ϕ_{ss} of a shaly sand containing equal volume fractions of illite and kaolinite is just the average of the two values of ϕ_{ss} corresponding to shaly sands containing only illite and only kaolinite. With an equivalent clean sandstone porosity, one can then obtain the value of $L_{s,mat}$ by treating it as equivalent to the $L_{s,mix}$ obtained using Eq. (4.1.3) with ϕ set equal to ϕ_{ss}. The equation for the equivalent clean sandstone porosity ϕ_{ss} is

$$\phi_{ss} = 0.132 f_{ill} + 0.412 f_{kao} \ , \tag{4.1.6}$$

where f_{ill} and f_{kao} are the volume fractions of illite and kaolinite, respectively, in the matrix. The equation used to obtain $L_{s,mat}$ for shaly sands is then

$$(L_{s,mat} - 4.5)^{\alpha} = (L_{s,w} - 4.5)^{\alpha}\phi_{ss} + (L_{s,ss} - 4.5)^{\alpha}(1 - \phi_{ss}) \ . \tag{4.1.7}$$

Since this is the "sandstone" equation, $a = -1.664$. Substituting in the values of α, $L_{s,ss}$, and $L_{s,w}$ and rearranging yields

$$L_{s,mat} = \left[0.00495(1 - \phi_{ss}) + 0.147(\phi_{ss})\right]^{-0.601} + 4.5 \ . \tag{4.1.8}$$

Although this procedure is somewhat complicated, it does provide the necessary tools to determine the porosity of a shaly sand if the measured value of the formation slowing down length and the volume fraction in the matrix and type of shale are known. Alternatively, if the porosity and slowing down length of a shaly sand are known, one can determine the bounds for the volume fraction of shale present. This will discussed further later.

At this point it seems appropriate to summarize the method. The overall governing mixing law is given by Eq. (4.1.3):

$$(L_{s,mix} - 4.5)^{\alpha} = (L_{s,w} - 4.5)^{\alpha}(\phi) + (L_{s,mat} - 4.5)^{\alpha}(1 - \phi) \ . \tag{4.1.3}$$

In order to use this law, one must know the values of both a and $L_{s,mat}$. Depending on what the matrix is, various methods are used to determine these parameters.

Case 1: Pure Matrices. Obtain a and $L_{s,mat}$ from the top four entries in Table 2.

Case 2: Matrix Mixtures Containing No Shale. Obtain a from Eq. (4.1.4):

$$a = \sum_{i=1}^{n} \alpha_i f_i \ . \qquad (4.1.4)$$

Obtain α_i's from the top four entries in Table 2. Obtain $L_{s,mat}$ from Eq. (4.1.5):

$$L_{s,mat} = 37.83\alpha^2 + 159.3\alpha + 188.75 \ . \qquad (4.1.5)$$

Case 3: Shaly Sands. Use $a = -1.664$, the value used for pure sandstone. Compute ϕ_{ss} using Eq. (4.1.6):

$$\phi_{ss} = 0.132\, f_{ill} + 0.412\, f_{kao} \ . \qquad (4.1.6)$$

Obtain $L_{s,mat}$ from Eq. (4.1.8):

$$L_{s,mat} = \left[0.00495(1 - \phi_{ss}) + 0.147\phi_{ss}\right]^{-0.601} + 4.5 \ . \qquad (4.1.8)$$

4.2. Comparison With Goertzel-Greuling Values

Comparisons between the slowing down length vs. porosity relationships as generated with the Goertzel-Greuling procedure and the same relationships as computed using the mixing law and procedures outlined previously are given at the end of this report in Figs. 12 through 38, one for each matrix considered. As these figures show, there is very good agreement between the two procedures. What is most important, however, is how the values of porosity as predicted by the two models compare to one another. Rearrangement of Eq. (4.1.3) yields the following expression for porosity:

$$\phi = \frac{(L_{s,mix} - 4.5)^{\alpha} - (L_{s,mat} - 4.5)^{\alpha}}{(L_{s,w} - 4.5)^{\alpha} - (L_{s,mat} - 4.5)^{\alpha}} \qquad (4.2.1)$$

Fig. 9 shows the comparisons between the two sets of values for the 14 matrices containing no shale and Fig. 10 shows the comparisons between the two sets of values for the 13 shaly sands. For both sets of matrices, the error for porosities of 30% or less are minor. Above 30% porosity, infrequently encountered in logging, the errors increase, but even at 40% porosi-

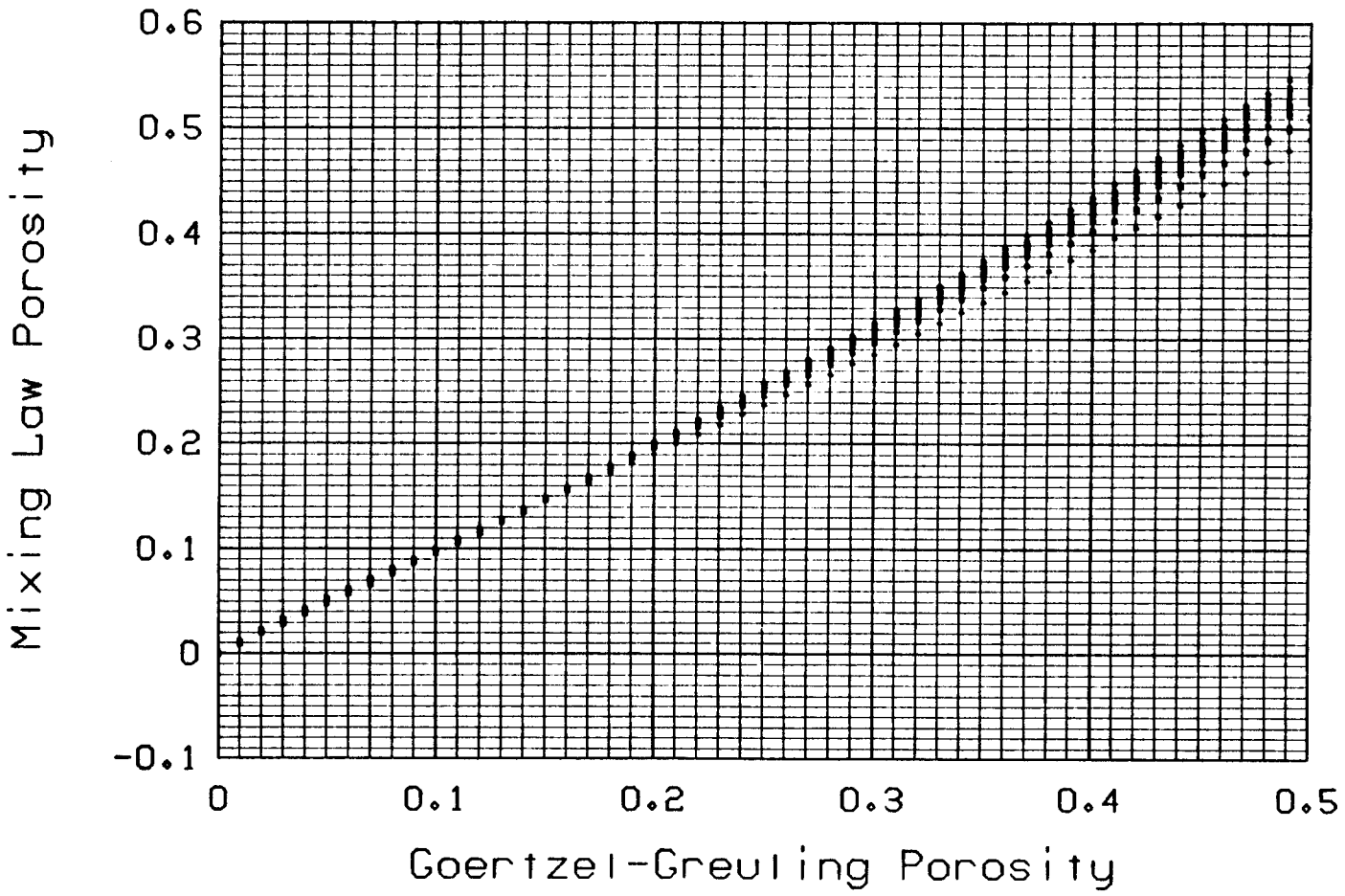

Figure 9. Mixing law porosity vs. Goertzel-Greuling porosity for the 14 non-shaly matrices listed in Table 2.

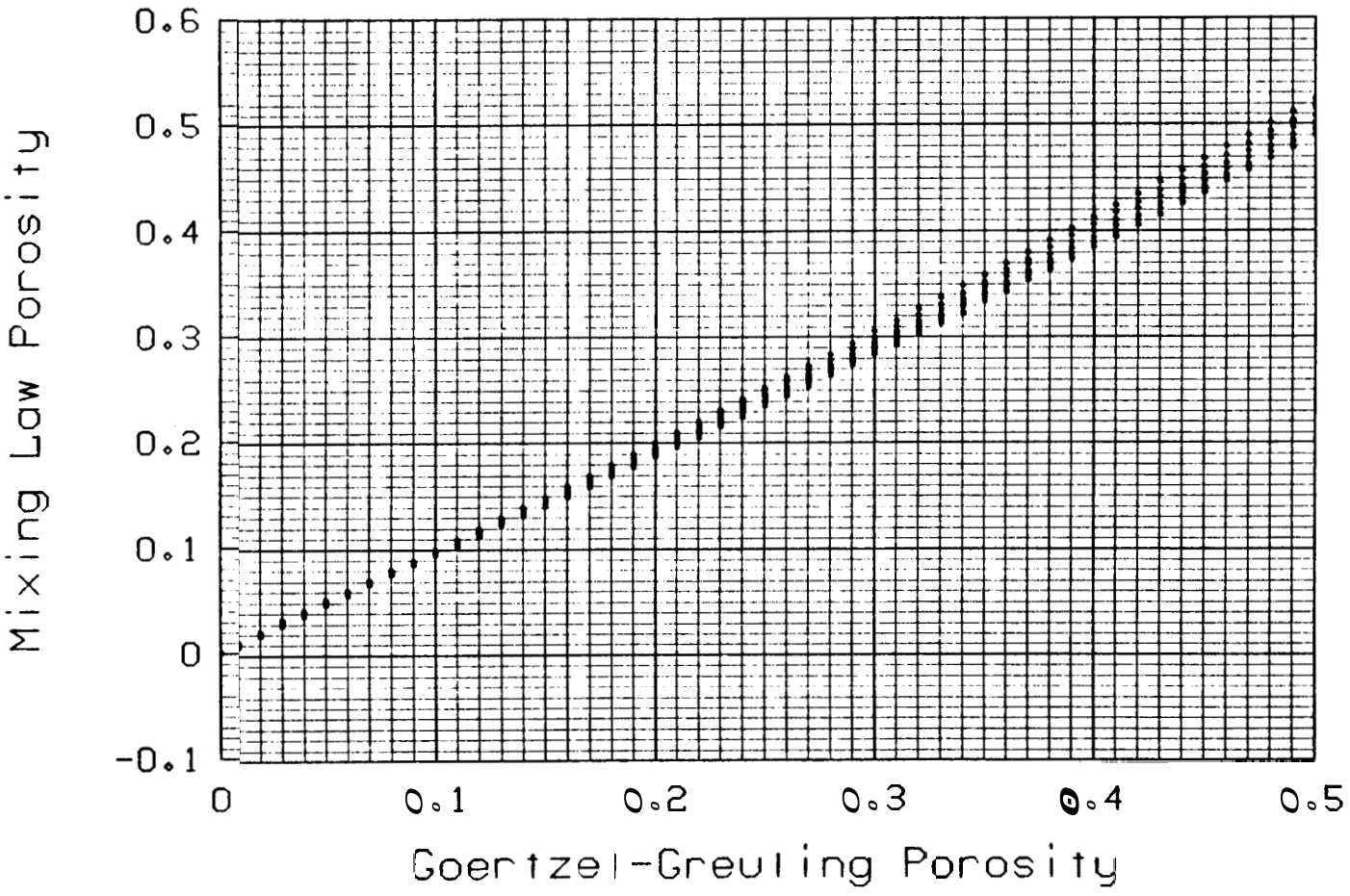

Figure 10. Mixing law porosity vs. Goertzel-Greuling porosity for the 13 shaly sands listed in Table 3.

ty they are mostly less than 2%.

43. Uses In Interpretation

As stated previously, the principal value of having a mixing law is that it allows the logging company to report the value of the quantity actually measured. This allows the log interpreter the option of interpreting the measurement directly. In cases where matrix mixtures or shale are encountered, this is especially important. Previously, when matrix mixtures were encountered, one could only estimate the porosity from the derived porosities of pure matrices; now, one can compute the actual porosity.

Additionally, one can use the mixing law and procedures outline previously to determine the limits of the matrix shale fraction in a shaly sand if the porosity is known from another source such as the density log or core measurements. If, in addition, the matrix shale fraction is known from another measurement such as Gamma Ray or aluminum activation, one can further quantify the amounts of shales containing four hydroxyls, such as illite, and eight hydroxyls, such as kaolinite. This is an important step in the clay typing process.

To show the use of the mixing law and procedures, a few examples are presented.

Example 1. Analysis of cuttings indicates that the matrix in the interval of interest is sandstone. The logging tool measures a slowing down length of 12.8 centimeters. From Table 2, $a = -1.664$ and $L_{s,mat} = 28.79$. From Table 1, $L_{s,w} = 7.67$. Using Eq. (4.2.1) porosity can be calculated as follows:

$$\phi = \frac{(12.8 - 4.5)^{-1.664} - (28.79 - 4.5)^{-1.664}}{(7.67 - 4.5)^{-1.664} - (28.79 - 4.5)^{-1.664}} , \qquad (4.3.1a)$$

or

$$\phi = 0.17 . \qquad (4.3.1b)$$

Example 2. Cuttings indicate that the matrix in the interval of interest is 40% dolomite and 60% limestone. The logging tool measures a slowing down length of 12.8 centimeters. Using Eqs. (4.1.4), (4.1.5), and (4.2.1) porosity can be calculated as follows:

First, determine a using Eq. (4.1.4):

$$a = (0.6)(-1.745) + (0.4)(-2.001) \ , \tag{4.3.2a}$$

or

$$a = -1.847 \ . \tag{4.3.2b}$$

Next, determine $L_{s,mat}$ using Eq. (4.1.5):

$$L_{s,mat} = (37.83)\ (-1.847)^2 + (159.3)\ (-1.847) + (188.75) \ , \tag{4.3.3a}$$

or

$$L_{s,mat} = 23.58\ cm \ . \tag{4.3.3b}$$

Finally, determine ϕ using Eq. (4.2.1):

$$\phi = \frac{(12.8 - 4.5)^{-1.847} - (23.58 - 4.5)^{-1.847}}{(7.67 - 4.5)^{-1.847} - (23.58 - 4.5)^{-1.847}} \ , \tag{4.3.4a}$$

or

$$\phi = 0.14 \ . \tag{4.3.4b}$$

Example 3. Cuttings indicate that the matrix in the interval of interest is a shaly sand containing 3% illite and 13% kaolinite. The logging tool measures a slowing down length of 12.8 centimeters. Using Eqs. (4.1.6), (4.1.8), and (4.2.1) porosity can be calculated as follows:

First, determine ϕ_{ss} using Eq. (4.1.6):

$$\phi_{ss} = (0.132)\ (0.03) + (0.412)\ (0.13) \ , \tag{4.3.5a}$$

or

$$\phi_{ss} = 0.0575 \ . \tag{4.3.5b}$$

Next, determine $L_{mat,s}$ using Eq. (4.1.8):

$$L_{s,mat} = \left[(0.00495)\ (1 - 0.0575) + (0.147)\ (0.0575)\right]^{-0.601} + 4.5 \ , \tag{4.3.6a}$$

or

$$L_{s,mat} = 18.06\,cm\ . \tag{4.3.6b}$$

Finally, determine ϕ using Eq. (4.2.1), with $a = -1.664$:

$$\phi = \frac{(12.8 - 4.5)^{-1.664} - (18.06 - 4.5)^{-1.664}}{(7.67 - 4.5)^{-1.664} - (18.06 - 4.5)^{-1.664}}\ , \tag{4.3.7a}$$

or

$$\phi = 0.12\ . \tag{4.3.7b}$$

Example 4. Figure 11 presents the log of a shaly sand. Track 3 on the far right displays the porosities as determined by the density tool (solid line) and the epithermal neutron tool (dotted line). Track 2 in the center displays the aluminum content as measured by the ACT* service. Because clay minerals are alumino-silicates, this measurement gives an indication of the amount of shale present. Track 1 on the left displays the amount of pure illite (solid line) or pure kaolinite (dotted line) necessary to explain the amount of shale present in the matrix. These curves were calculated with knowledge of just the slowing down length and porosity of the formation. The slowing down length of the formation was calculated from the ratio of the detector rates as shown in Eq. (3.4.5) and the porosity was obtained from the density log. The slowing down length of the matrix $L_{s,mat}$ was then calculated using Eq. (4.1.3). Next, the equivalent clean sandstone porosity ϕ_{ss} was calculated with Eq. (4.1.8). Finally, Eq. (4.1.6) was used to calculate the curves in Track 1 by setting one of the shale fractions to zero and calculating the other.

The separation between the density- and epithermal-derived porosities indicates the presence of shale. In Fig. 11, the interval from 2310' to 2375' is less shaly than the interval from 2418' to 2494' and the interval from 2375' to 2418' contains nearly pure shale. The curves in Track 1 indicate that if the shale is pure illite, there must be a large amount present. Con-

*mark of Schlumberger

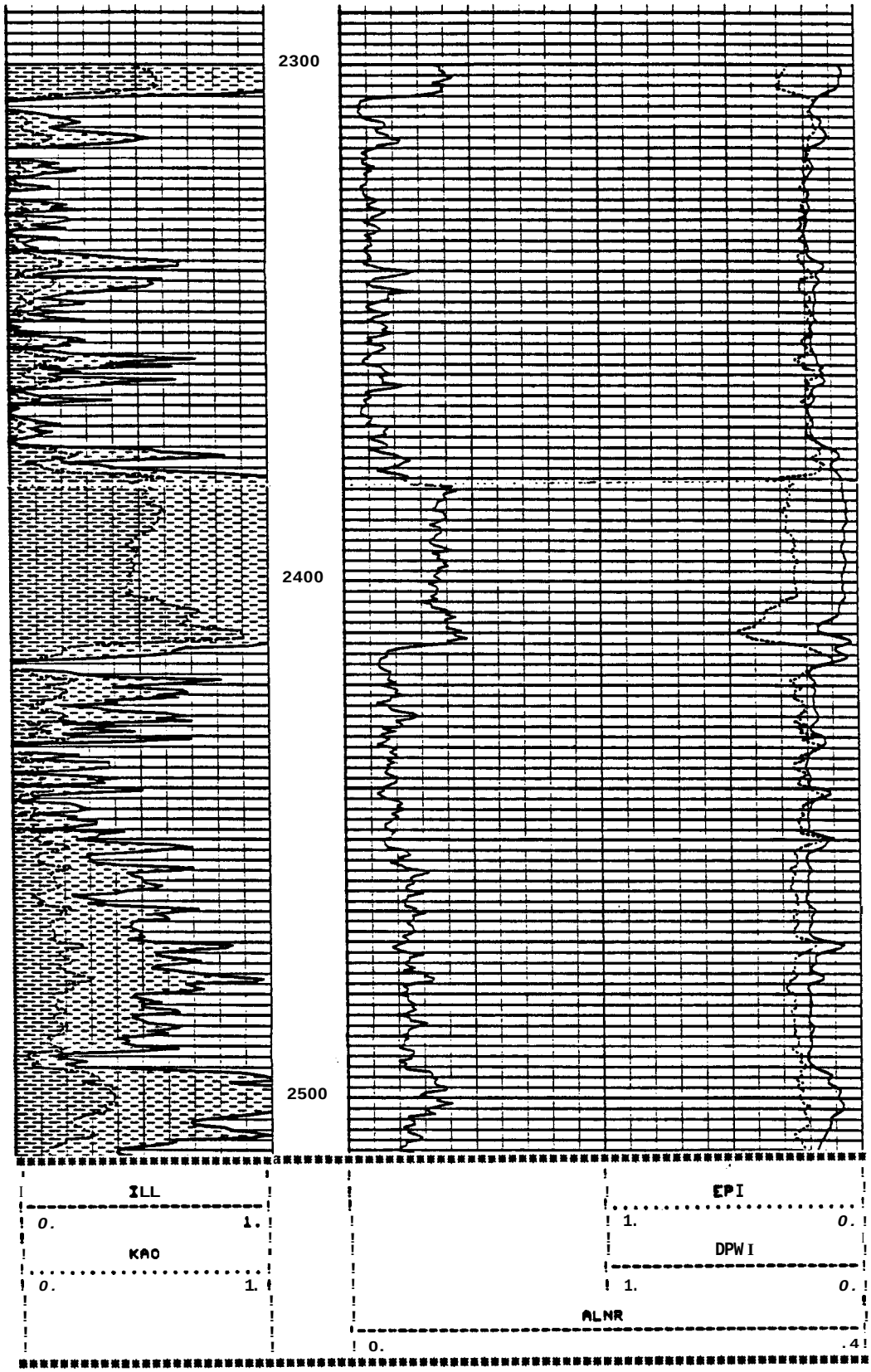

Figure 11. Log through a shaly sand interval, with curves in Track 1 indicating volume fractions of illite and kaolinite necessary to produce the differences between the neutron- and density-derived porosities indicated in Track 3.

versely, if the shale is pure kaolinite, the shale fraction is not as high. The interval around 2500' is not a pure shale. Since the illite curve indicates that it would take a matrix containing 100% illite to produce the neutron-derived porosity indicated, one can infer that the shale must contain at least some kaolinite-type shale. Most shales contain a mixture of the two shale types, i.e., of the $(OH)_2$ types and the $(OH)_8$ types. With knowledge of the total shale fraction, the individual shale type fractions can be calculated, because Eq. (4.1.6) gives one equation containing the two variables, and another equation is that the sum of the two fractions must equal the total shale fraction.

Another point of interest in Fig. 11 is the behavior of the curves in the interval from 2375' to 2418'. Although the total shale content remains relatively constant, as indicated by the aluminum curve, the amount of kaolinite-type shale changes significantly at 2404'. Finally, the kaolinite curve represents the minimum amount of shale present in the matrix. If the kaolinite fraction is less than the fraction indicated by that curve, then the illite fraction must compensate by being greater than the amount of kaolinite replaced.

5. CONCLUSIONS

A new technique for interpreting neutron log data has been developed. The neutron logging tool measures the neutron detection rates of two detectors and converts the ratio of the two detection rates to the porosity of a clean sandstone, limestone, or dolomite. The ratio of the detection rates is dependent upon a property of the formation known as the slowing down length.

A volumetric mixing law has been determined for slowing down length. If one has knowledge of the matrix type and the slowing down length of the formation, this law and the accompanying procedures can be used to determine the porosity. Whereas previous interpretation could be done only for pure matrices, this law can also be applied to shaly sands and matrix mixtures such as limestone/dolomite or even a matrix mixture consisting of sandstone, limestone, dolomite, and anhydrite. Additionally, if the porosity of a shaly sand is known from another source, the procedure can be used to determine upper and lower limits of the volume fraction of shale in the matrix. Finally, if the shale type is known to be either illite or kaolinite, the volume fraction of that shale in the matrix can be determined accurately; likewise, if the volume fraction of shale in the matrix is known from another independent measurement, the amounts of the two shale types (those containing four hydroxyls and those containing eight hydroxyls) can be calculated.

NOMENCLATURE

A	=	atomic mass
D	=	thermal diffusion coefficient
C	=	conductivity
E	=	energy
f	=	volume fraction
g	=	any physical property
i	=	$\sqrt{-1}$
k	=	a constant
L	=	length
N_A	=	Avagadro's Number
P_e	=	photoelecmc index
Q	=	neutron point source strength
R	=	resistivity
r	=	source to detector distance
S	=	saturation
At	=	interval transit time
U	=	macroscopic gamma ray cross section
v	=	velocity
Z	=	atomic number
α	=	exponent in general mixing formula
γ	=	gamma ray
ε	=	dielectric constant
θ	=	departure angle in elastic collisions
λ	=	mean free path
ρ	=	density
Σ	=	macroscopic neutron cross section
σ	=	neutron cross section
Φ	=	neutron detector count rate
ϕ	=	porosity
ω	=	frequency

Subscripts

b	=	bulk
c	=	compressional wave
d	=	diffusion
e	=	electron
ep	=	epithermal
f	=	fluid
i	=	corresponding to type i or component i
ill	=	illite
kao	=	kaolinite
log	=	from the log
m	=	migration
mat	=	mamx
mix	=	mixture
s	=	slowing down
ss	=	equivalent clean sandstone
th	=	thermal
w	=	water

REFERENCES

1. Asquith, George B.: ***Basic Well Log Analysis For Geologists,*** **AAPG,** Tulsa **(1982) 67.**

2. Korvin, ***G.:*** "Axiomatic Characterization of the General **Mixture** Rule," ***Geoexploration*** (June **1982) 267-76.**

3. Schlumberger: ***Log Interpretation, Volume I--Principles,*** **1972** edition, Schlumberger Limited, New York City **(1972) 45.**

4. Wyllie, M.R.J., Gregory, A.R., and Gardner, G.H.F.: "Elastic Wave Velocities in Heterogeneous and Porous Media," ***Geophysics*** (Jan. **1956) 41-70.**

5. Hearst, Joseph R., and Nelson, Philip H.: ***Well Logging for Physical Properties,*** McGraw-Hill Book Co., New York City **(1985) 14.**

6. Bertozzi, W., Ellis, D.V., and Wahl, J.S.: "The Physical Foundation of Formation Lithology Logging with Gamma Rays," ***Geophysics*** (Oct. **1981) 1439-55.**

7. Tittle, C.W.: "Theory of Neutron Logging I," ***Geophysics*** (Feb. **1961) 27-39.**

8. Tittle, C.W., and Allen, L.S.: "Theory of Neutron Logging **II,**" ***Geophysics*** (Feb. **1966) 214-24.**

9. Allen, **L.S.,** Tittle, C.W., Mills, W.R., and Caldwell, R.L.: "Dual-Spaced Neutron Logging for Porosity," ***Geophysics*** (Feb. **1967) 60-68.**

10. Ellis, Darwin V.: ***Well Logging for Earth Scientists,*** Elsevier Scientific Publishing Co., New York City, to **be** published.

11. Hearst, Joseph R., and Nelson, Philip H.: ***Well Logging for Physical Properties,*** McGraw-Hill Book Co., New York City **(1985) 240-60.**

12. Kreft, A.: "Calculation of the Neutron Slowing Down Length in Rocks and Soils," ***Nukleonika*** (Feb. **1974) 145-56.**

13. Ellis, Darwin **V.:** "Neutron Porosity Devices--What **Do** They Measure?" ***First Break*** (March **1986) 11-17.**

14. Edmundson, H., and Raymer, L.L.: "Radioactive Logging Parameters for Common Minerals," ***Trans. Soc. Prof Well Log Analysts 20th Logging Symp.*** **(1979)** paper ***O.***

15. Beckurts, K.H., and Wirtz, K.: ***Neutron Physics,*** Springer-Verlag, New York City **(1964) 130-31.**

16. IMSL, Inc.: "Subroutine **ZXSSQ,"** ***The IMSL Library, Vol. 4,*** ninth edition, IMSL, Inc. **(1982)** Section **ZXSSQ.**

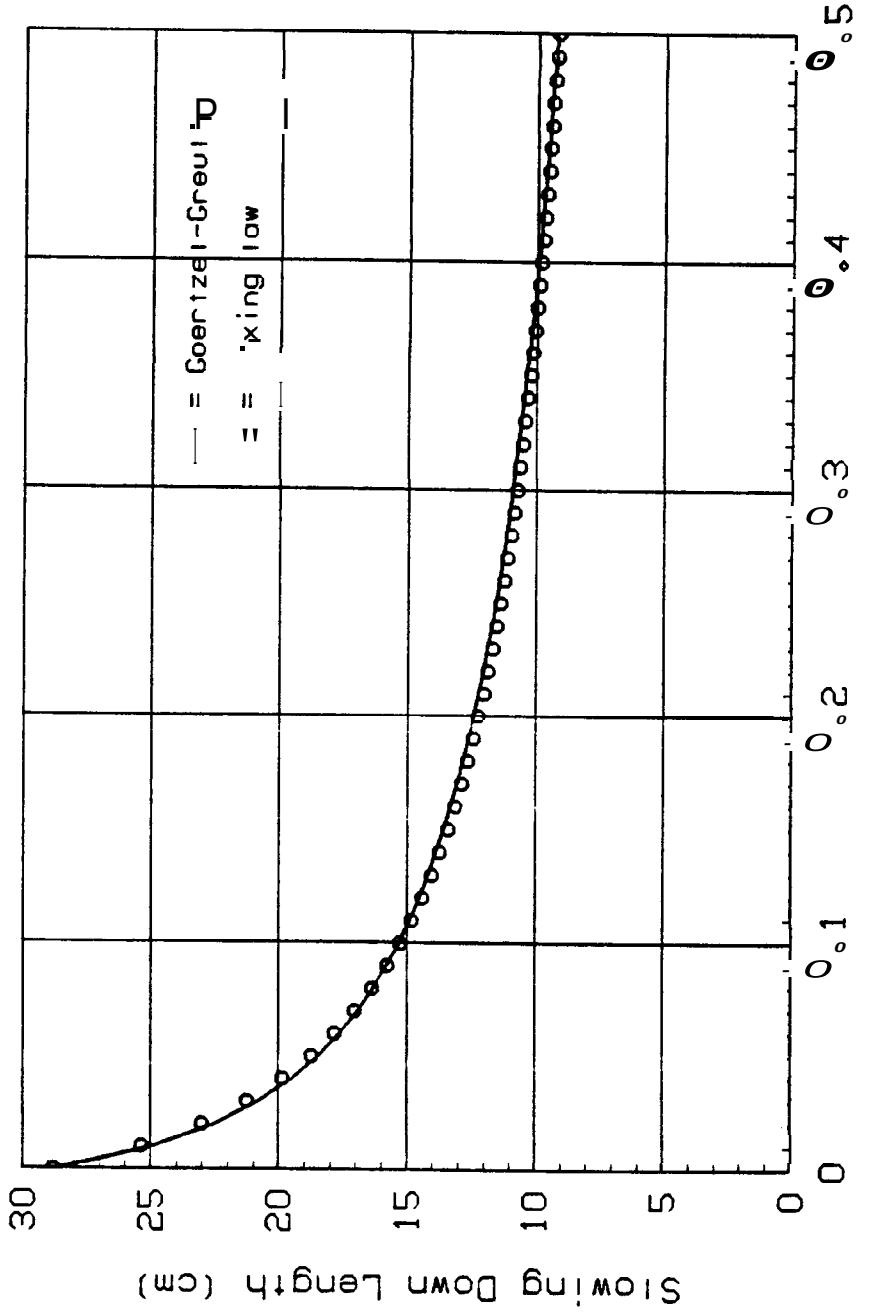

Figure 12. Slowing down length vs. water-filled porosity as predicted by two models indicated for matrix of 100% sandstone.

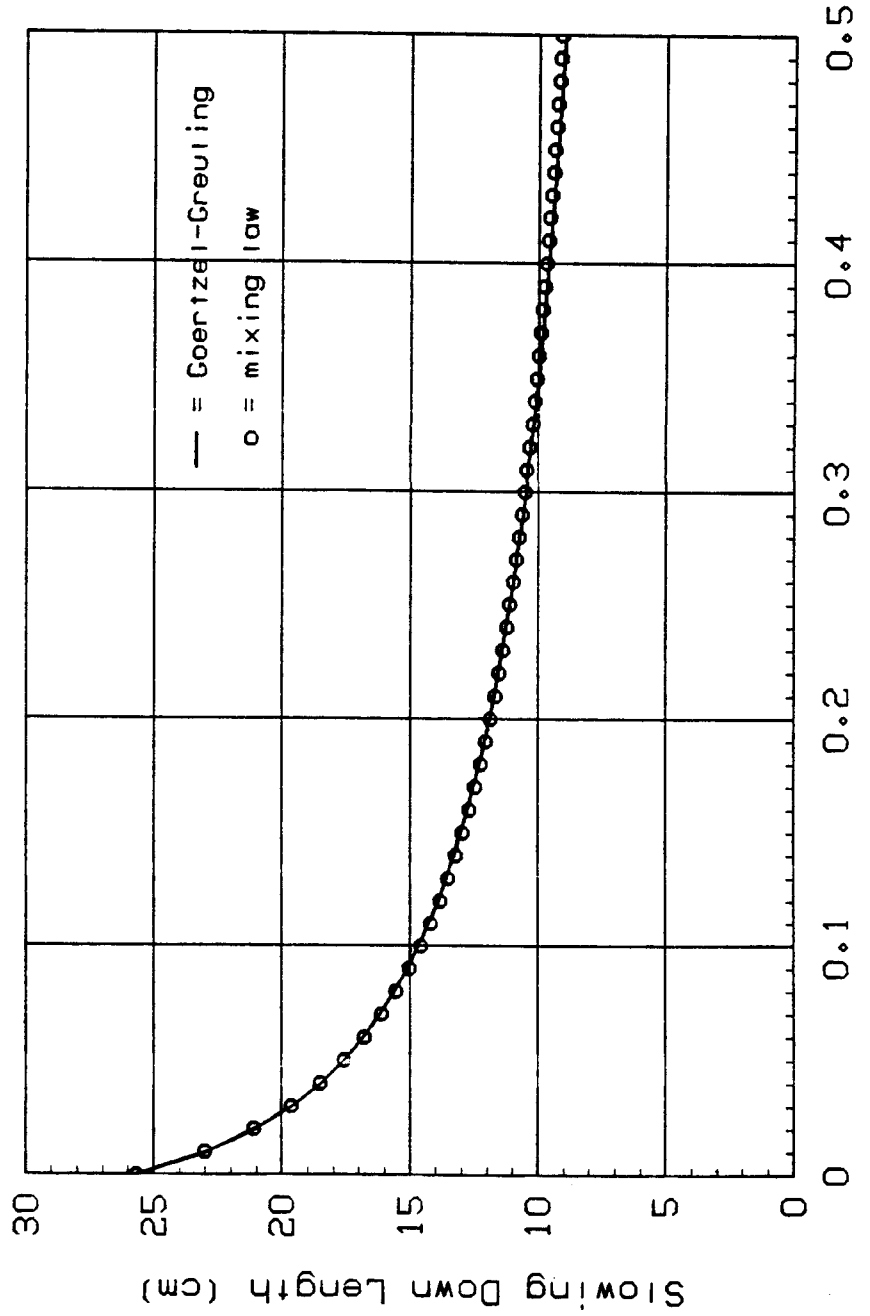

Figure 13. Slowing down length vs. water-filled porosity as predicted by two models indicated for matrix of 100% limestone.

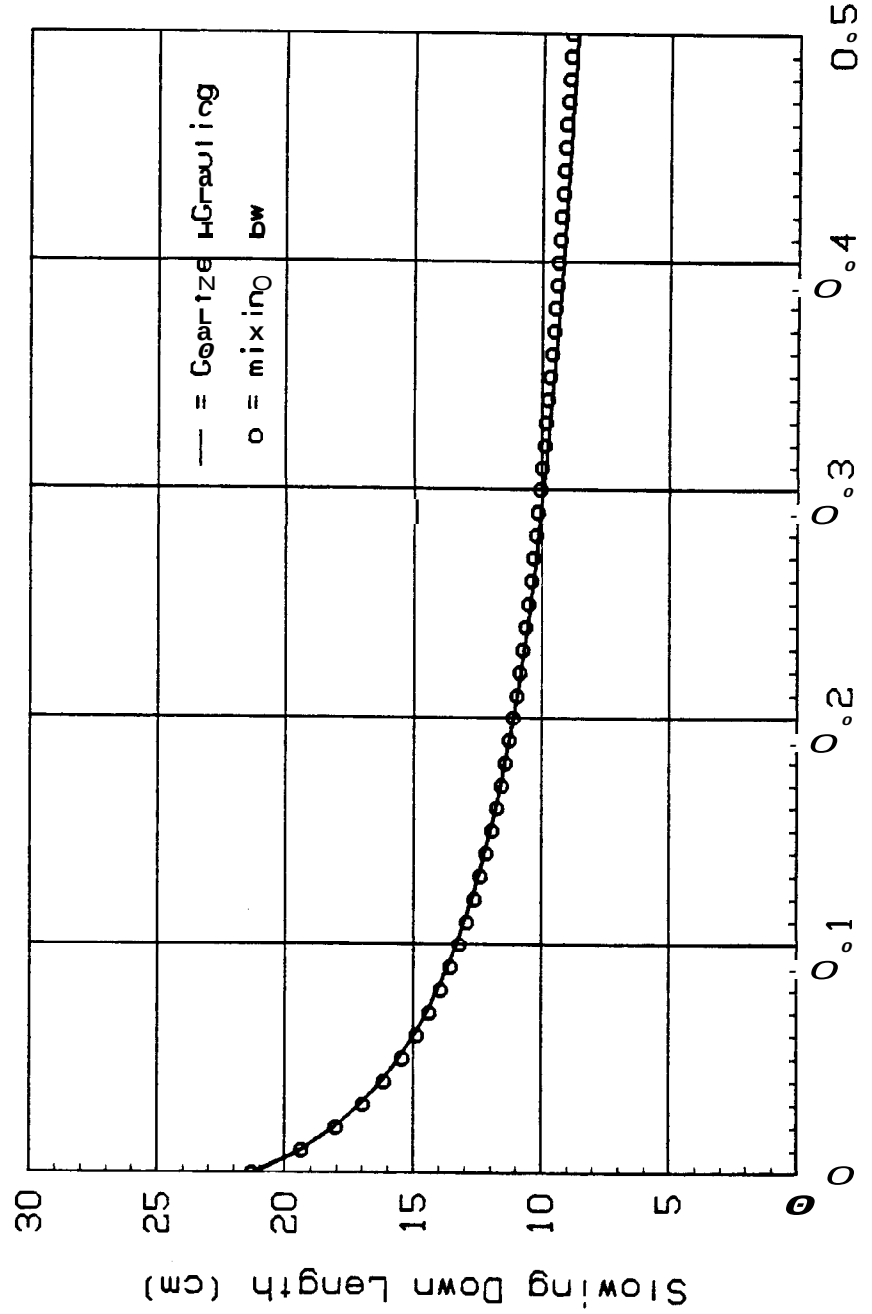

Figure 14. Slowing down length vs. water-filled porosity as predicted by two models indicated for matrix of 100% dolomite.

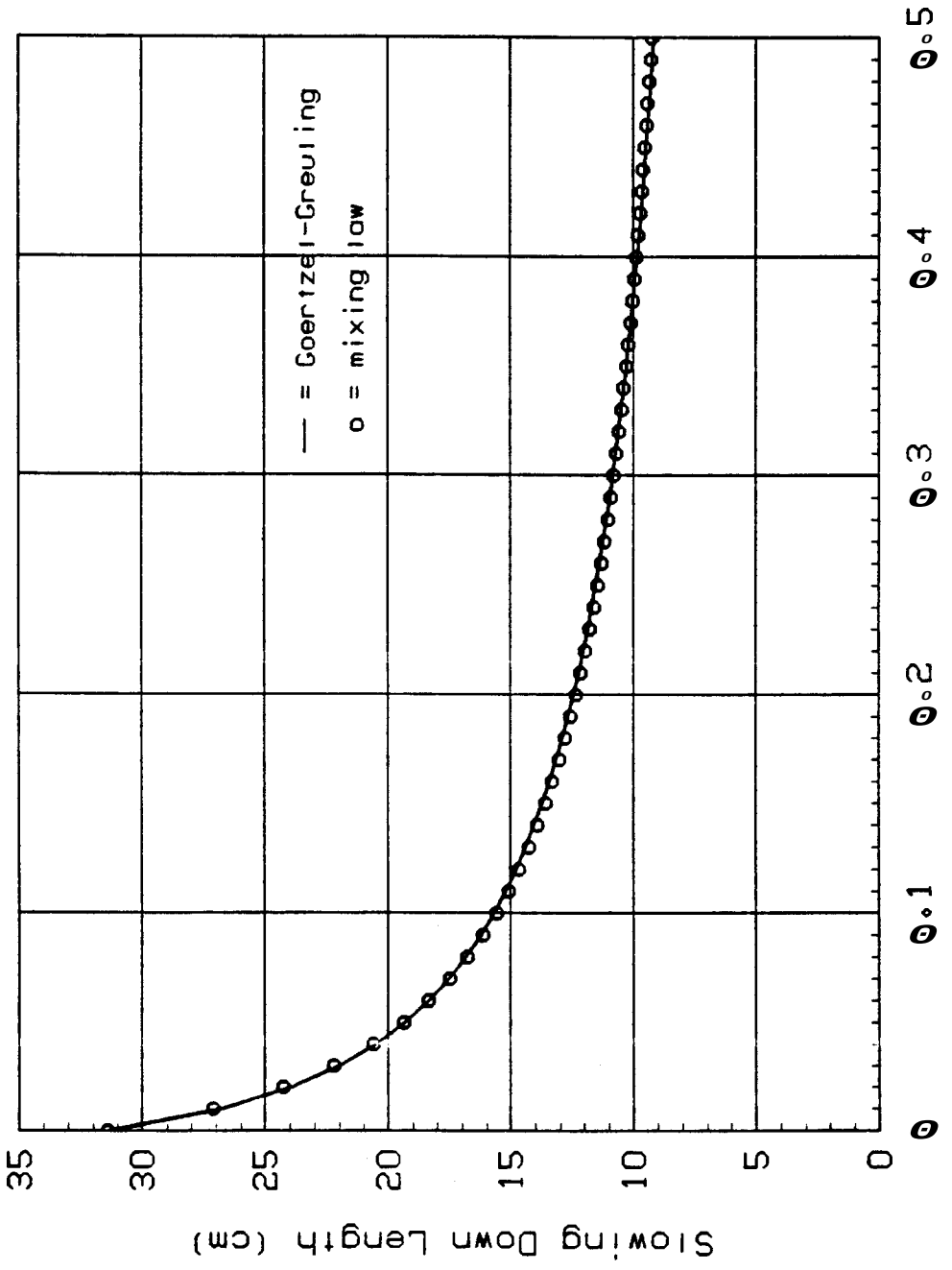

Figure 15. Slowing down length vs. water-filled porosity as predicted by two models indicated for matrix of 100% anhydrite.

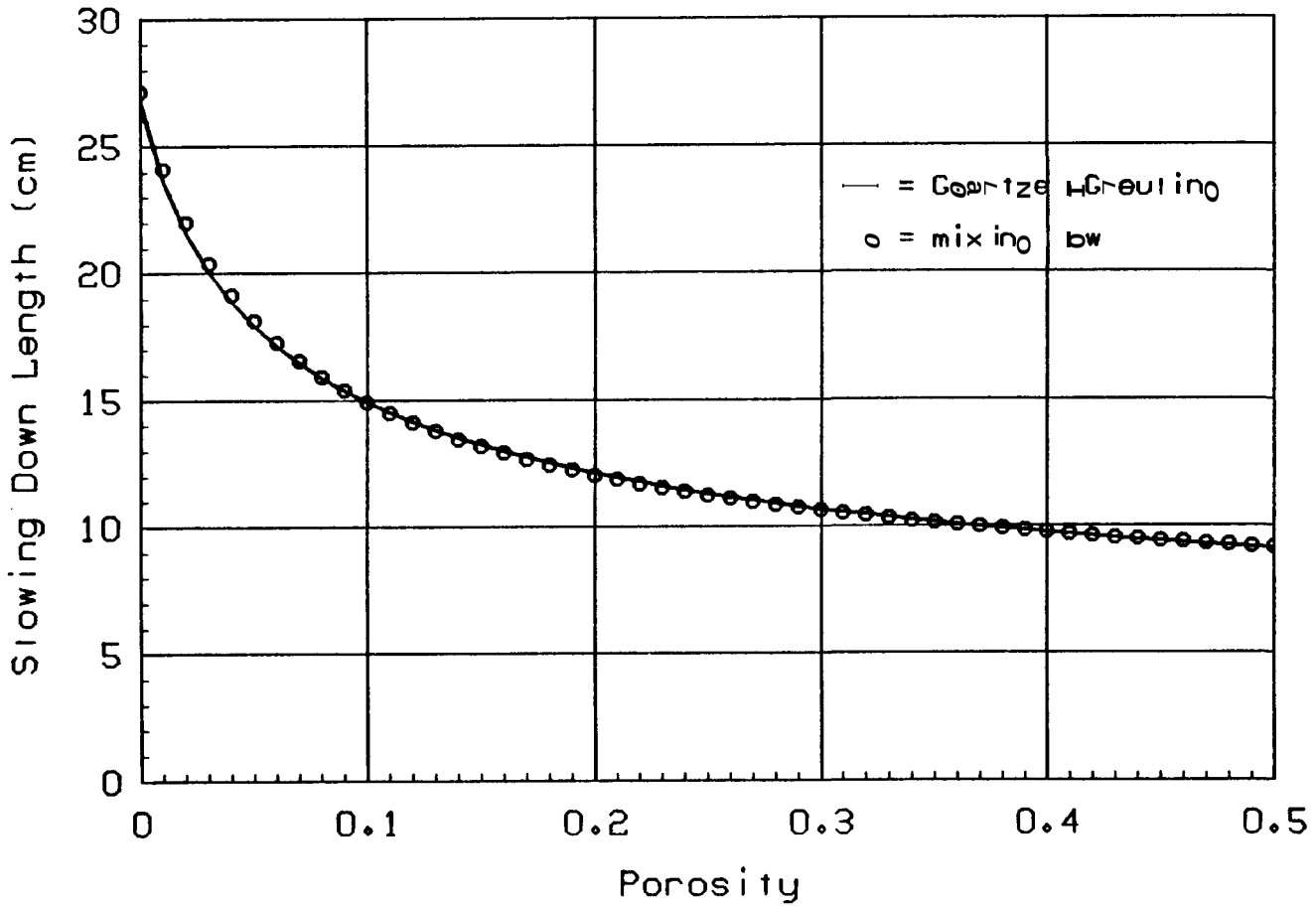

Figure 16. Slowing down length vs. water-filled porosity as predicted by two models indicated for matrix of 50% sandstone, 50% limestone.

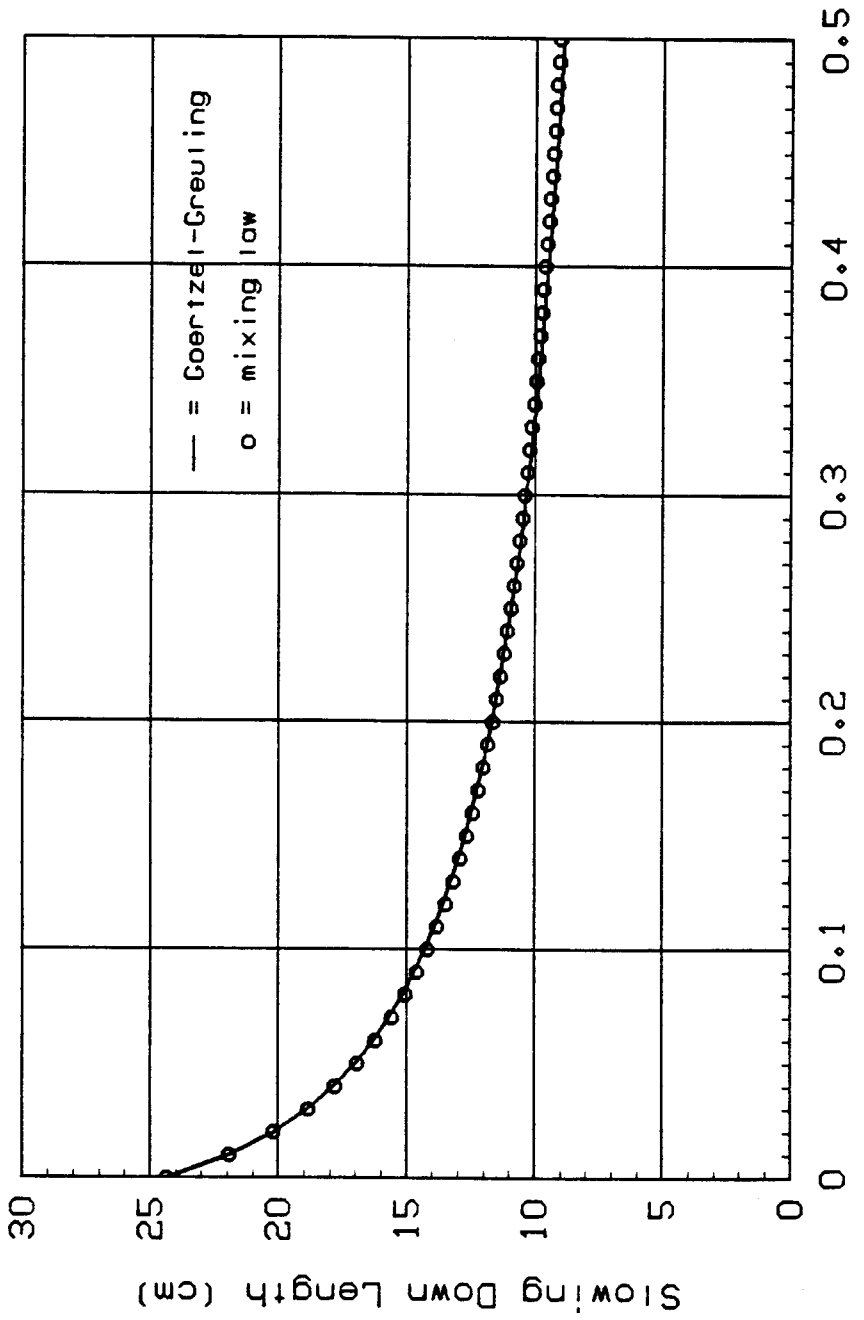

Figure 17. Slowing down length vs. water-filled porosity as predicted by two models indicated for matrix of 75% limestone, 25% dolomite.

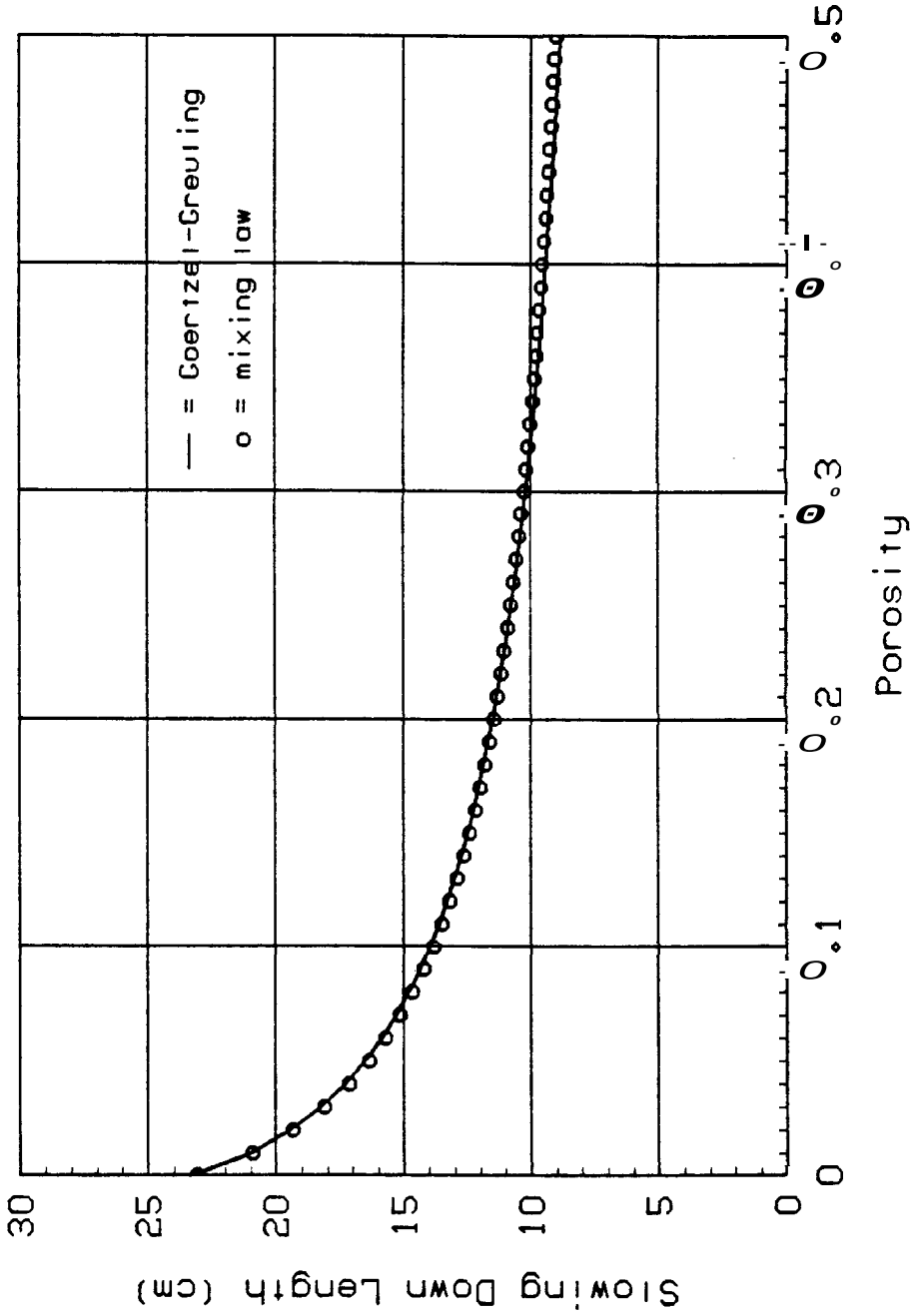

Figure 18. Slowing down length vs. water-filled porosity as predicted by two models indicated for matrix of 50% limestone, 50% dolomite.

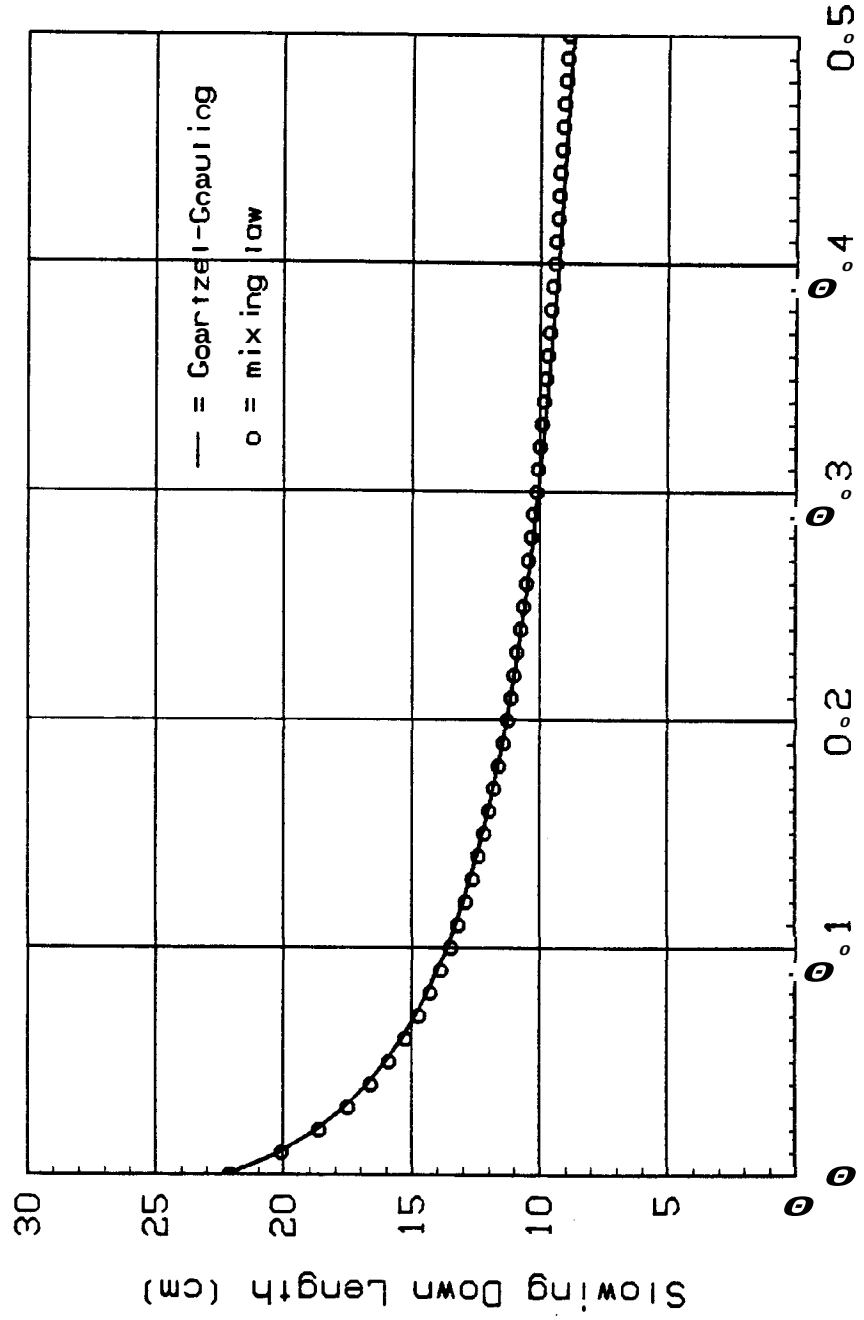

Figure 19. Slowing down length vs. water-filled porosity as predicted by two models indicated for matrix of 25% limestone, 75% dolomite.

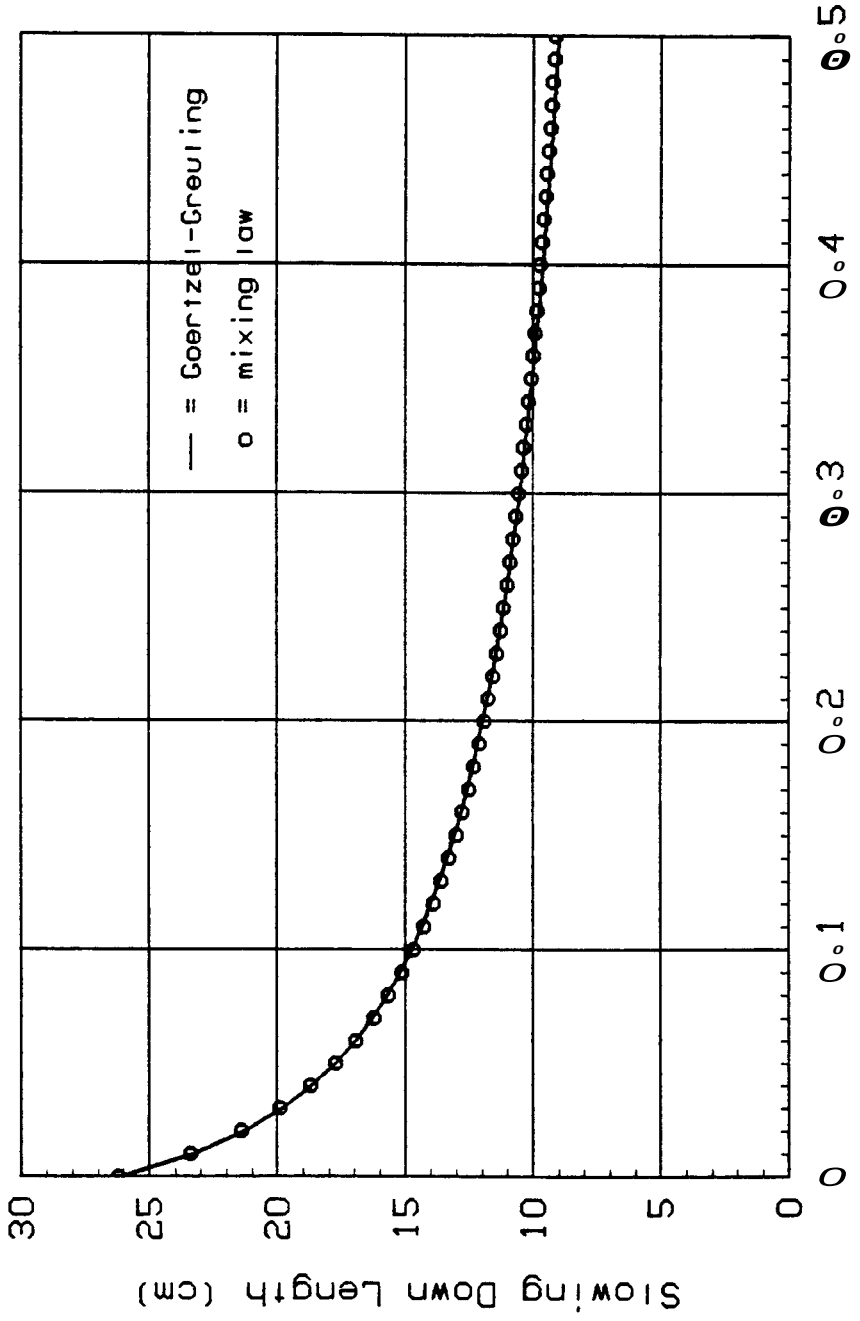

Figure 20. Slowing down length vs. water-filled porosity as predicted by two models indicated for matrix of 90% limestone, 10% anhydrite.

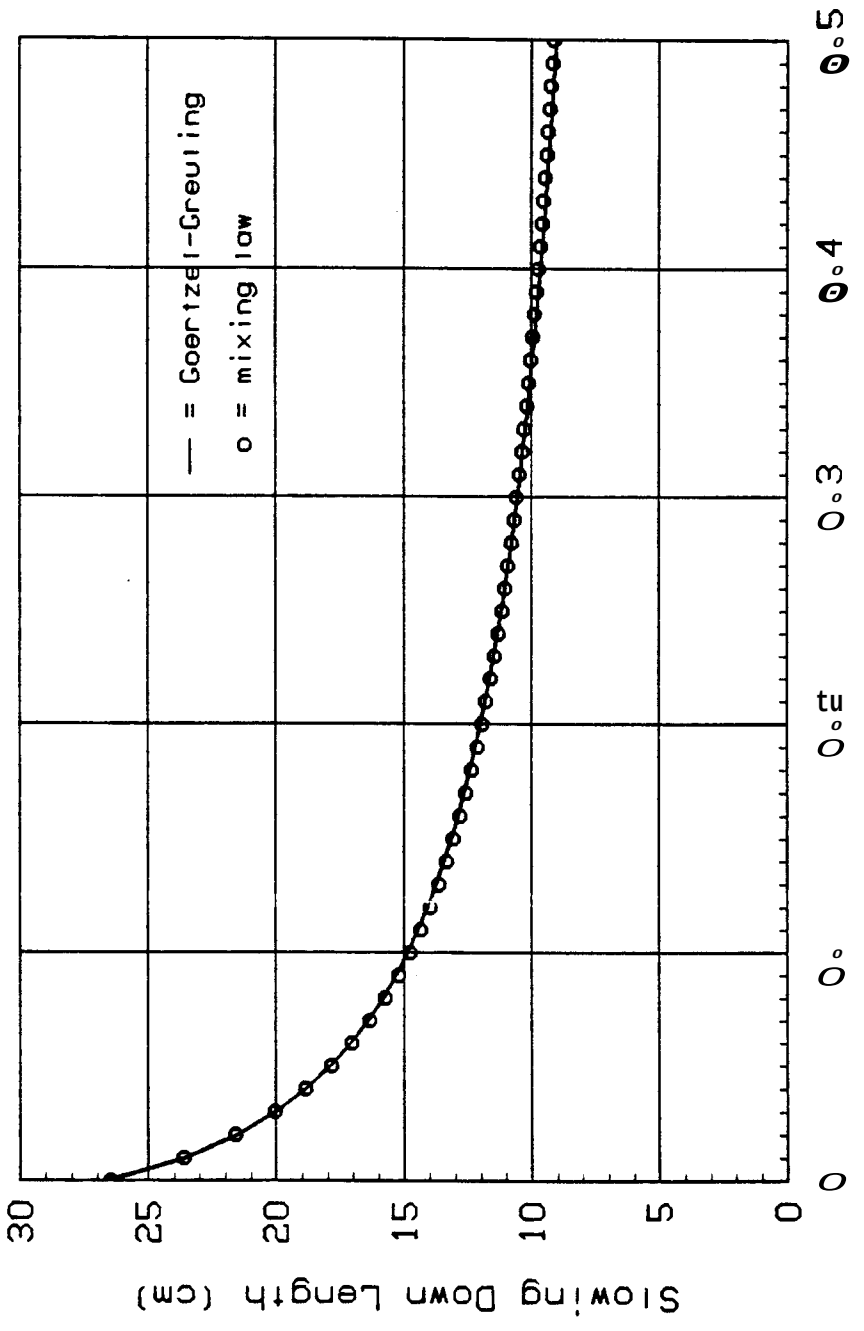

Figure 21. Slowing down length vs. water-filled porosity as predicted by two models indicated for matrix of 80% limestone, 20% anhydrite.

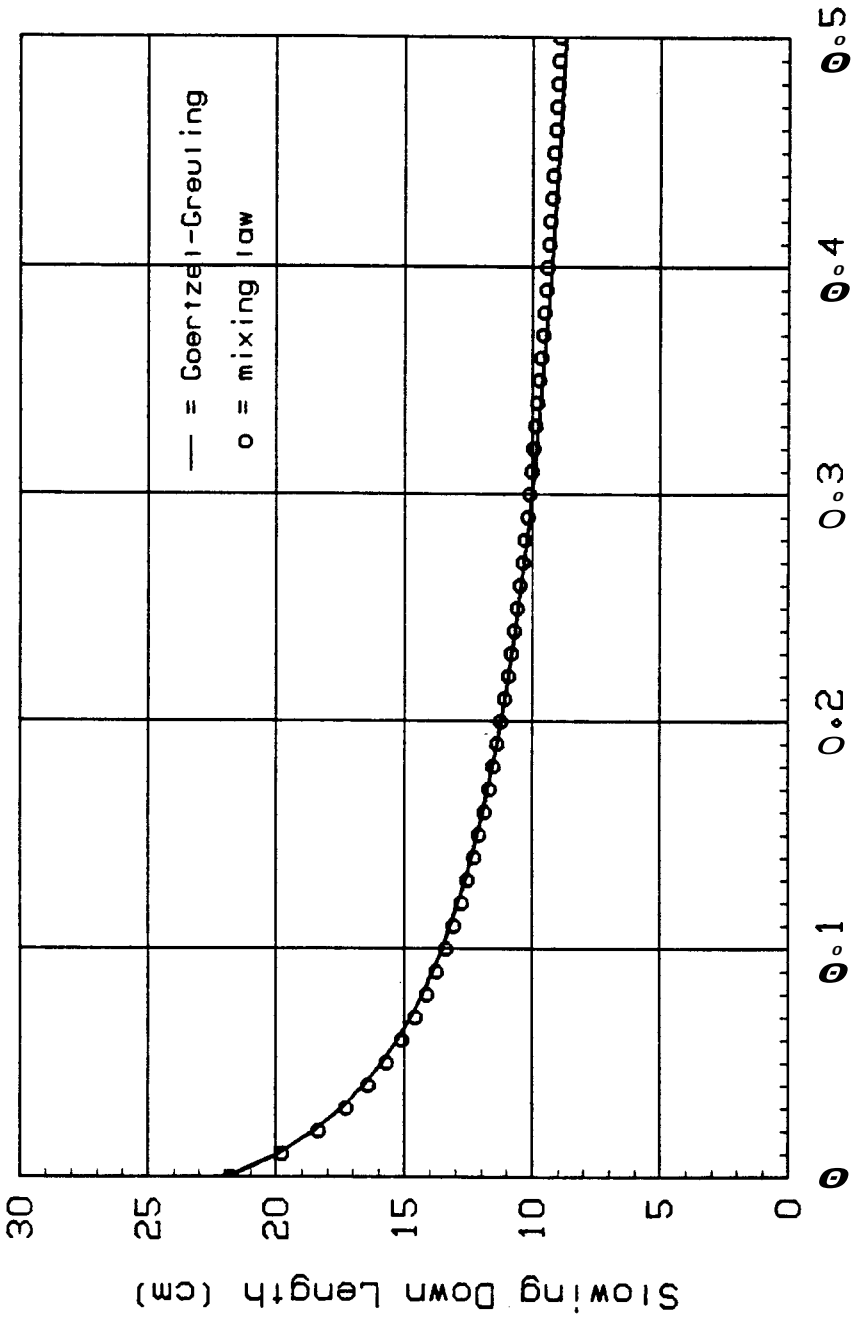

Figure 22. Slowing down length vs. water-filled porosity as predicted by two models indicated for matrix of 90% dolomite, 10% anhydrite.

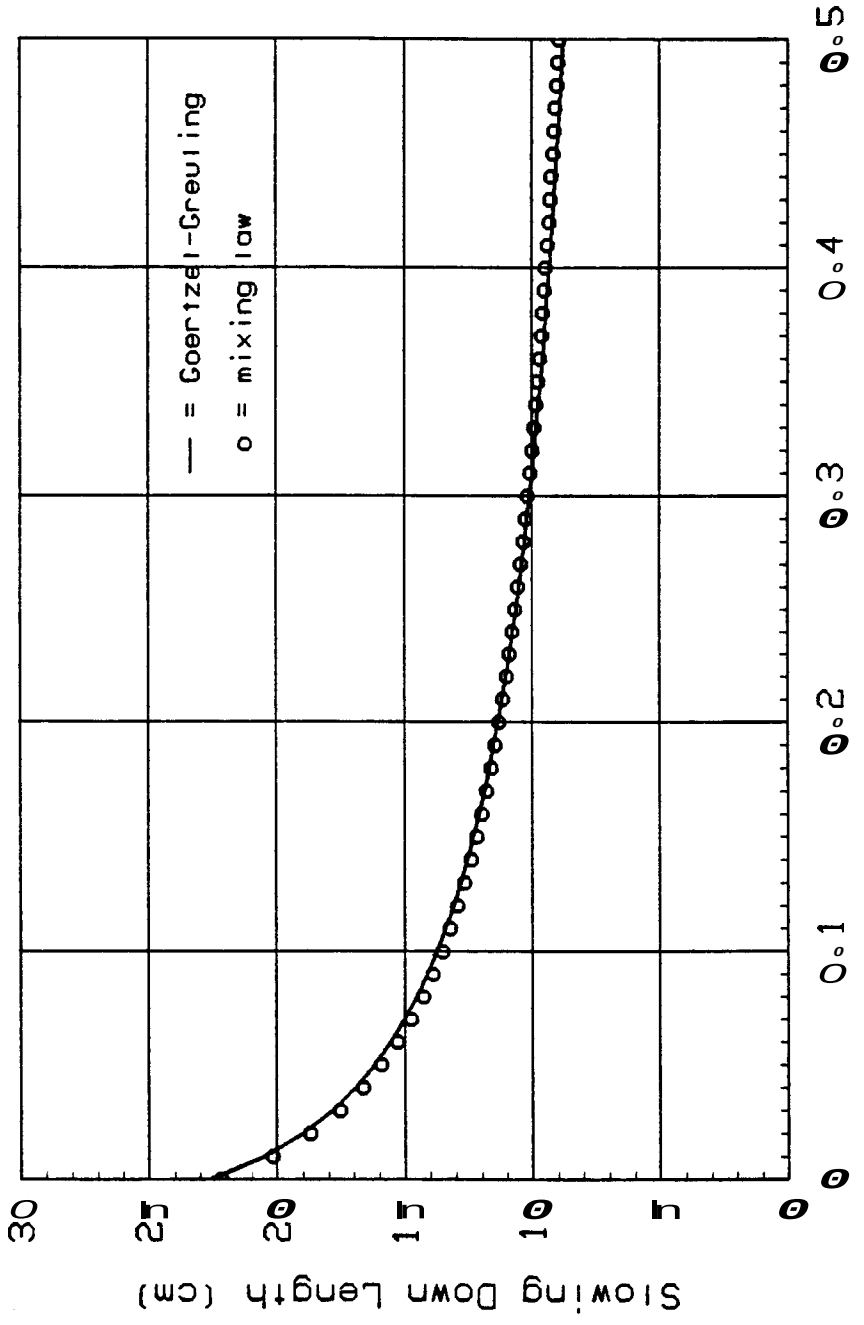

Figure 23. Slowing down length vs. water-filled porosity as predicted by two models indicated for matrix of 80% dolomite, 20% anhydrite.

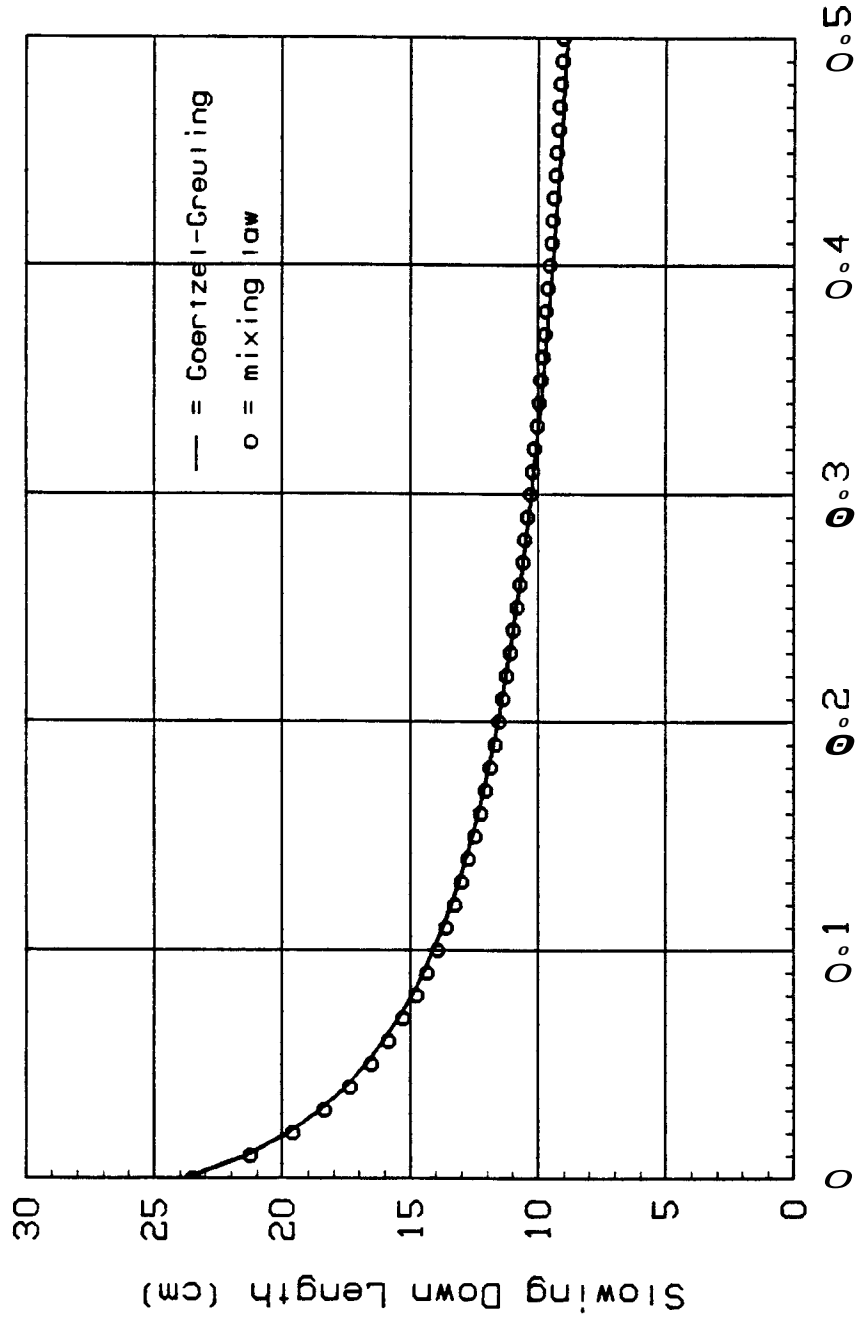

Figure 24. Slowing down length vs. water-filled porosity as predicted by two models indicated for matrix of 45% limestone, 45% dolomite, 10% anhydrite.

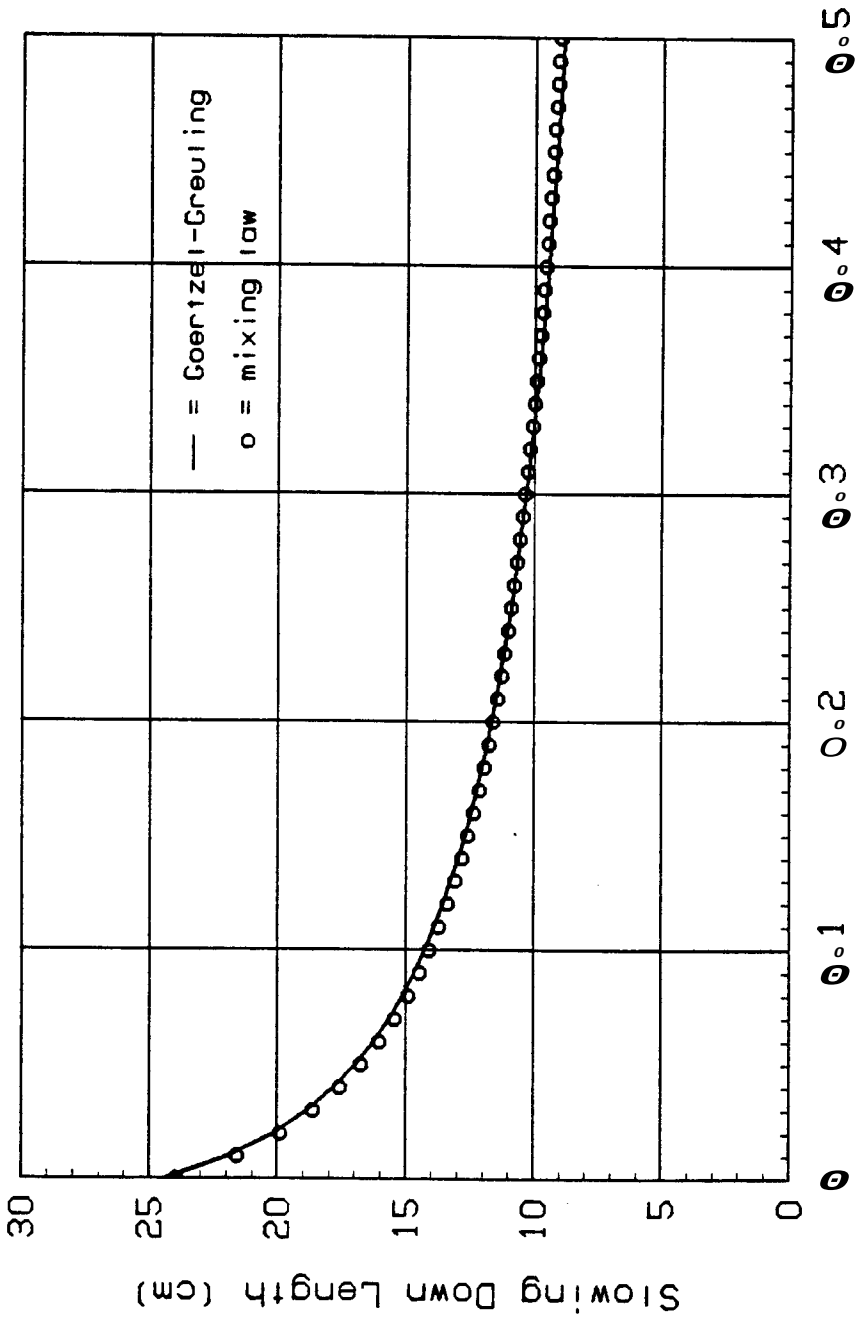

Figure 25. Slowing down length vs. water-filled porosity as predicted by two models indicated for matrix of 40% limestone, 40% dolomite, 20% anhydrite.

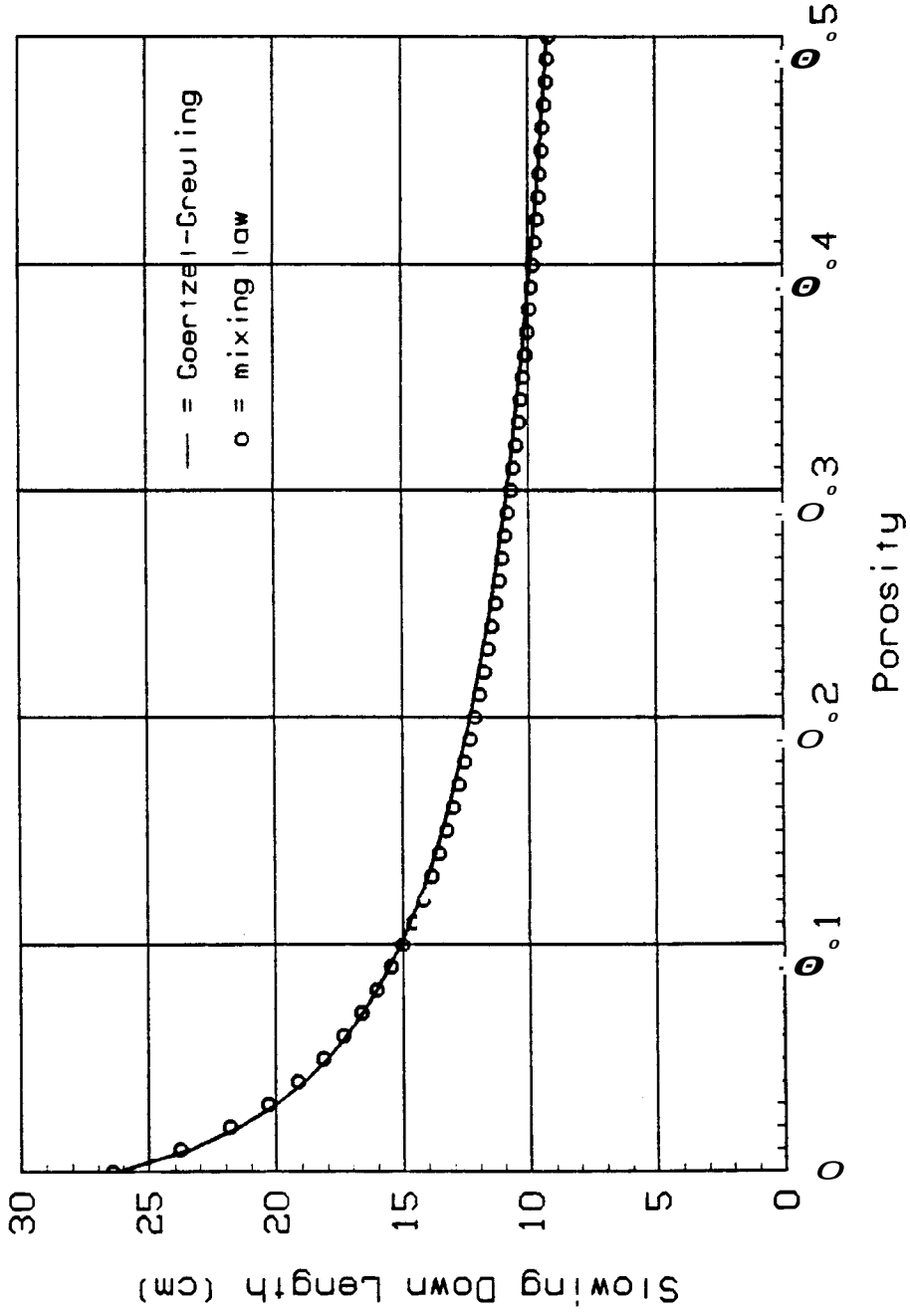

Figure 26. Slowing down length vs. water-filled porosity as predicted by two models indicated for matrix of 95% sandstone, 5% illite.

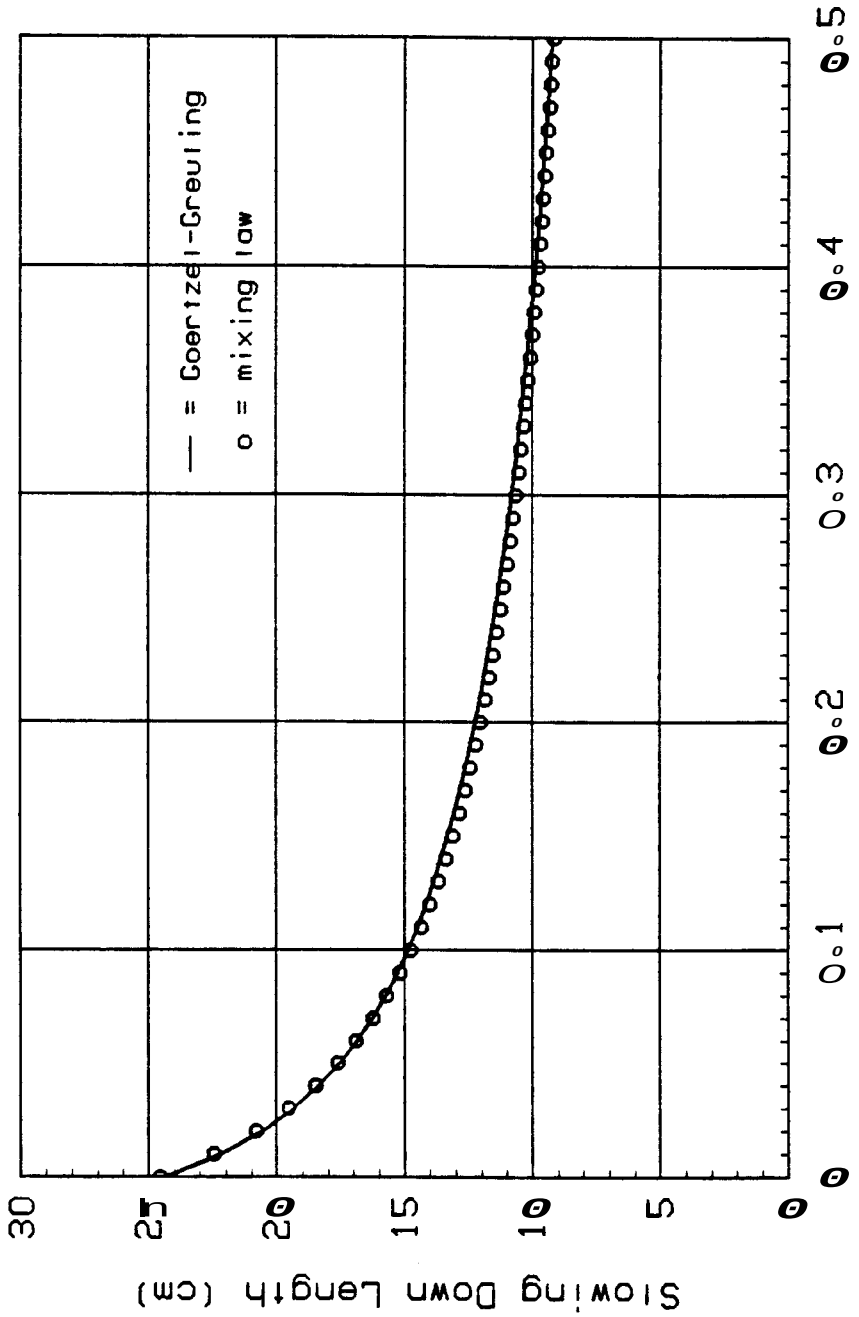

Figure 27. Slowing down length vs. water-filled porosity as predicted by two models indicated for matrix of 90% sandstone, 10% illite.

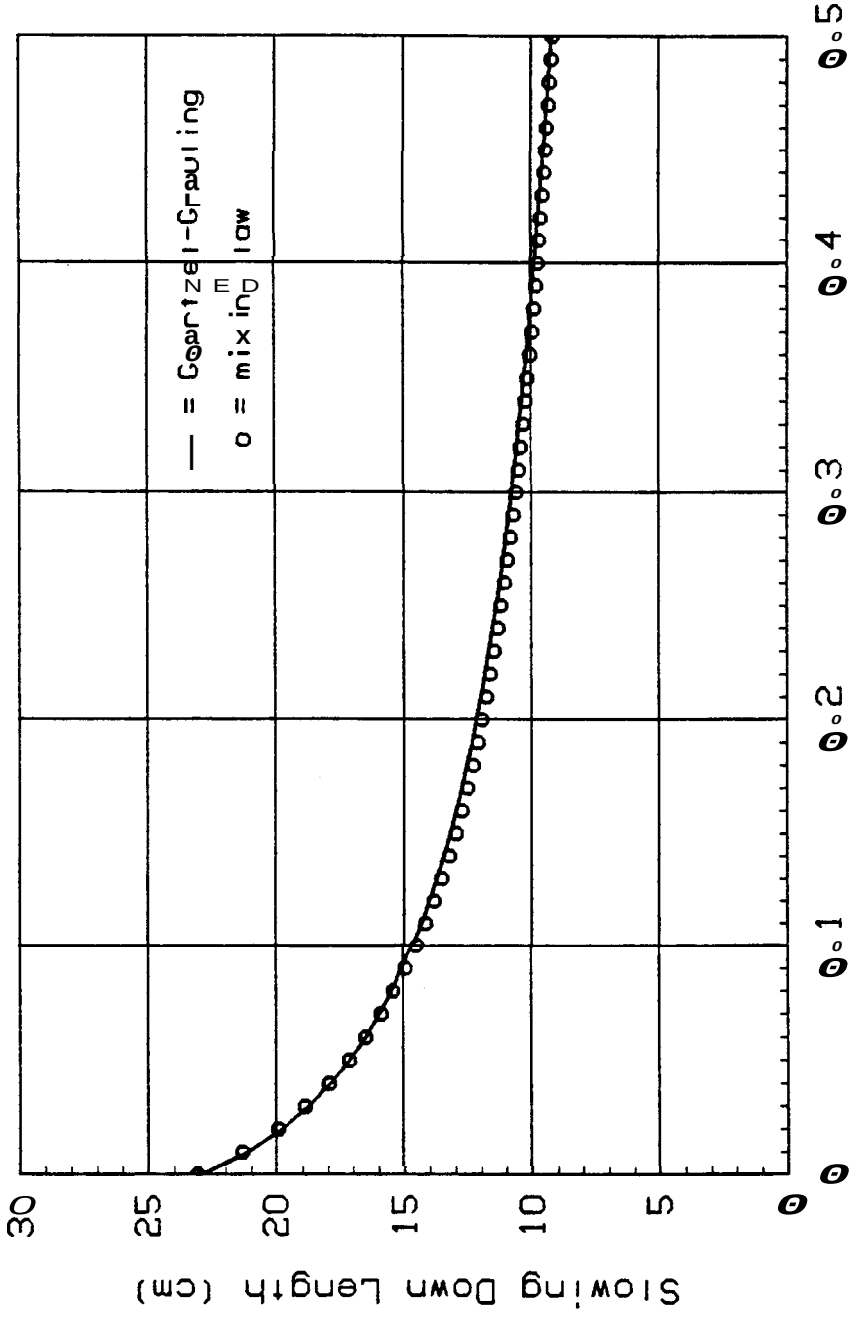

Figure 28. Slowing down length vs. water-filled porosity as predicted by two models indicated for matrix of 85% sandstone, 15% illite.

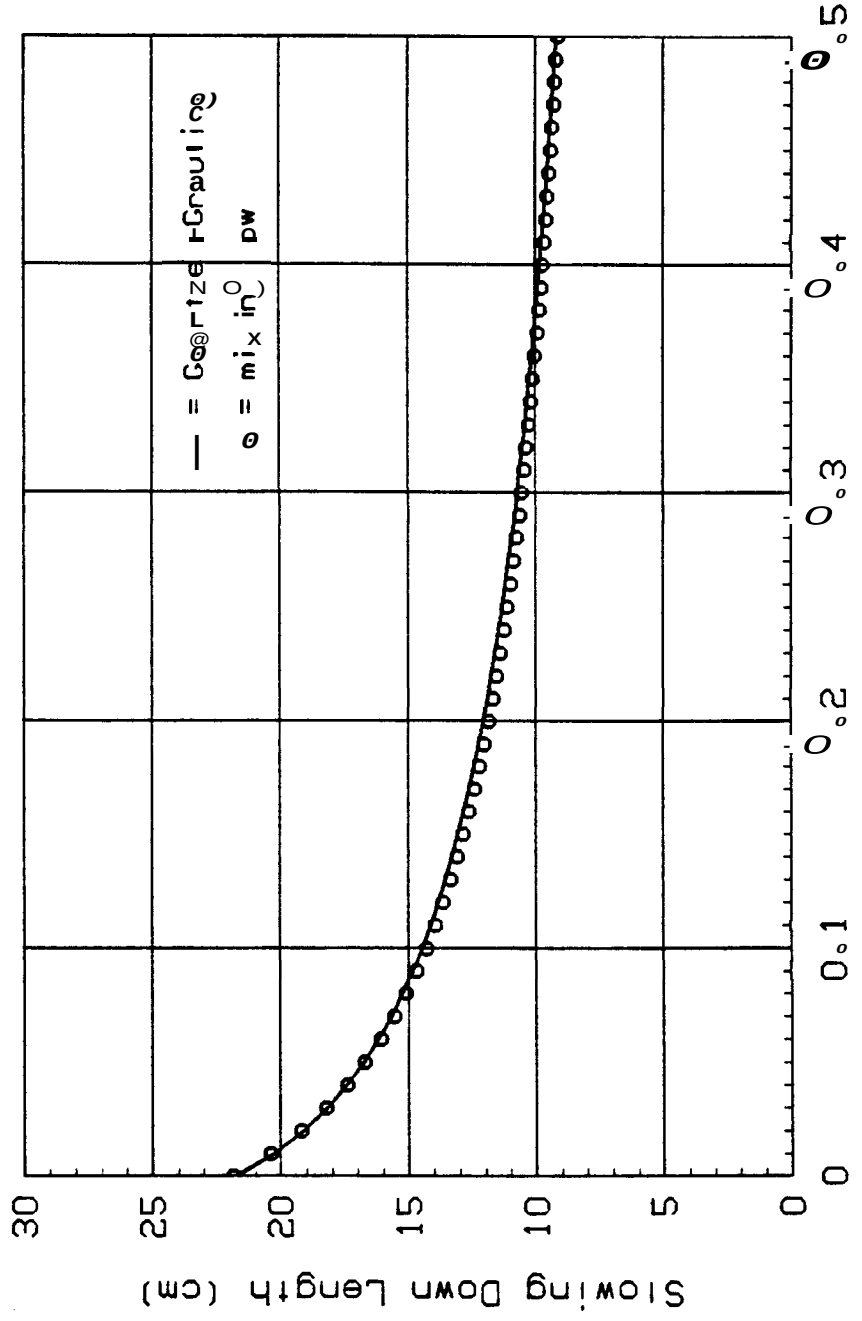

Figure 29. Slowing down length vs. water-filled porosity as predicted by two models indicated for matrix of 80% sandstone, 20% illite.

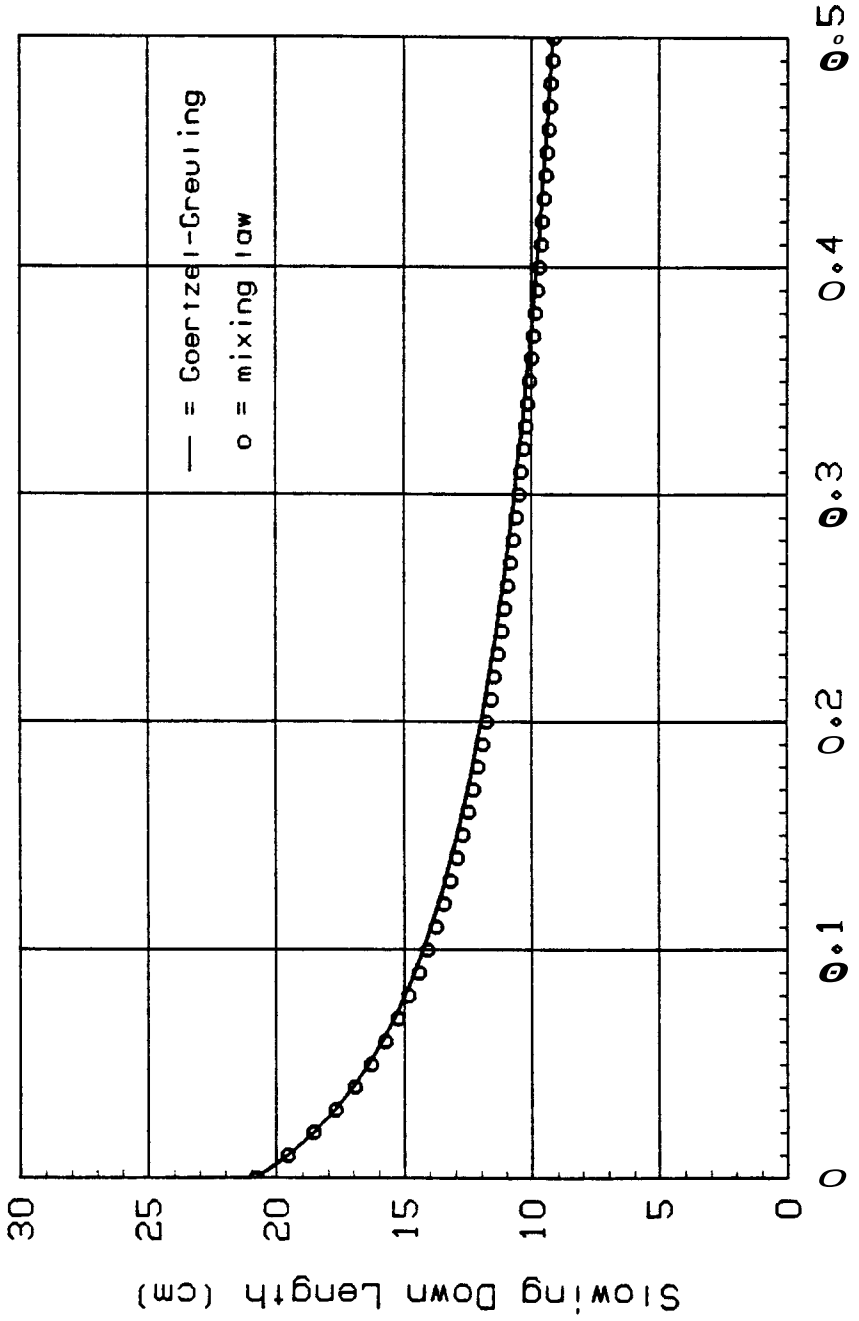

Figure 30. Slowing down length vs. water-filled porosity as predicted by two models indicated for matrix of 75% sandstone, 25% illite.

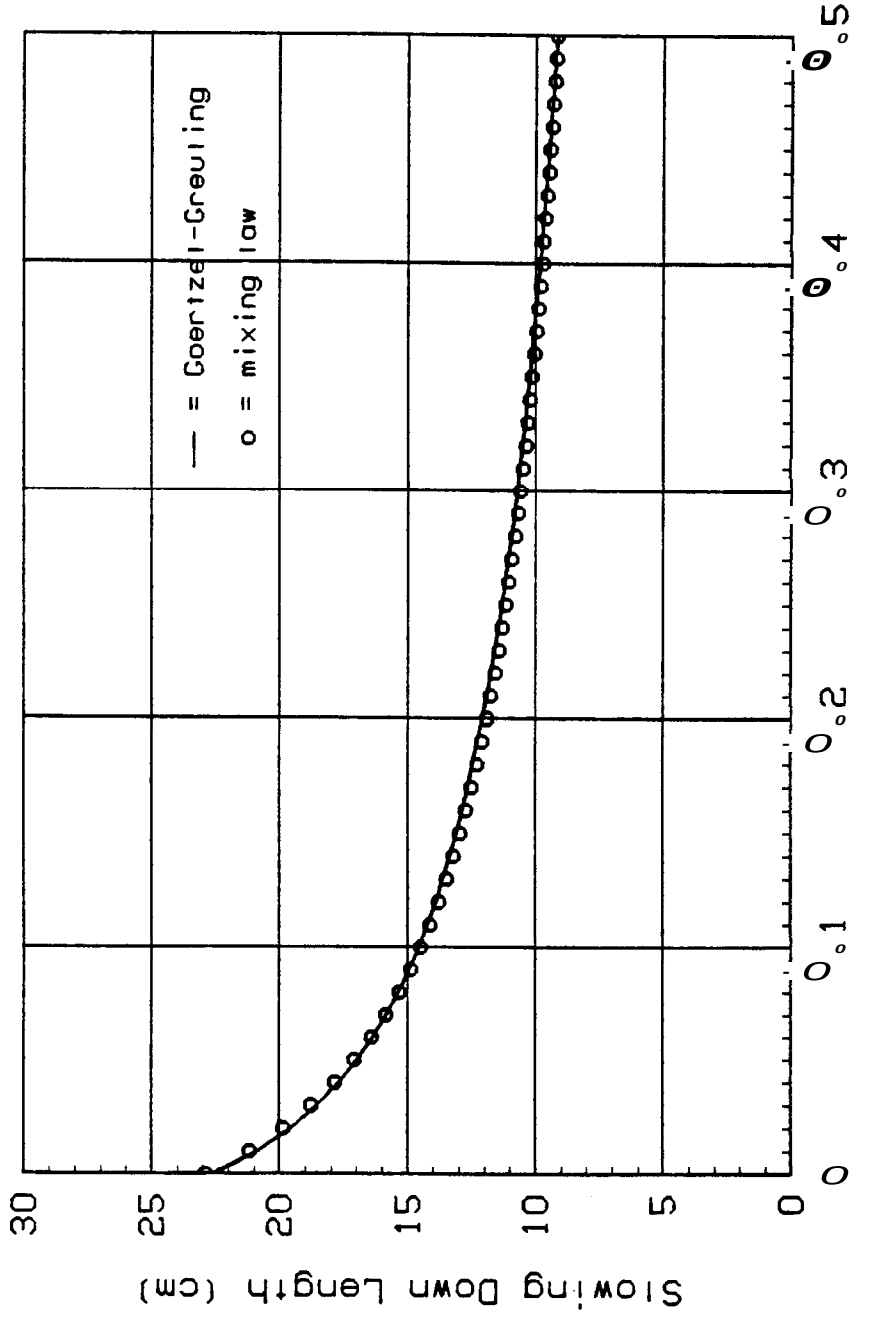

Figure 31. Slowing down length vs. water-filled porosity as predicted by two models indicated for matrix of 95% sandstone, 5% kaolinite.

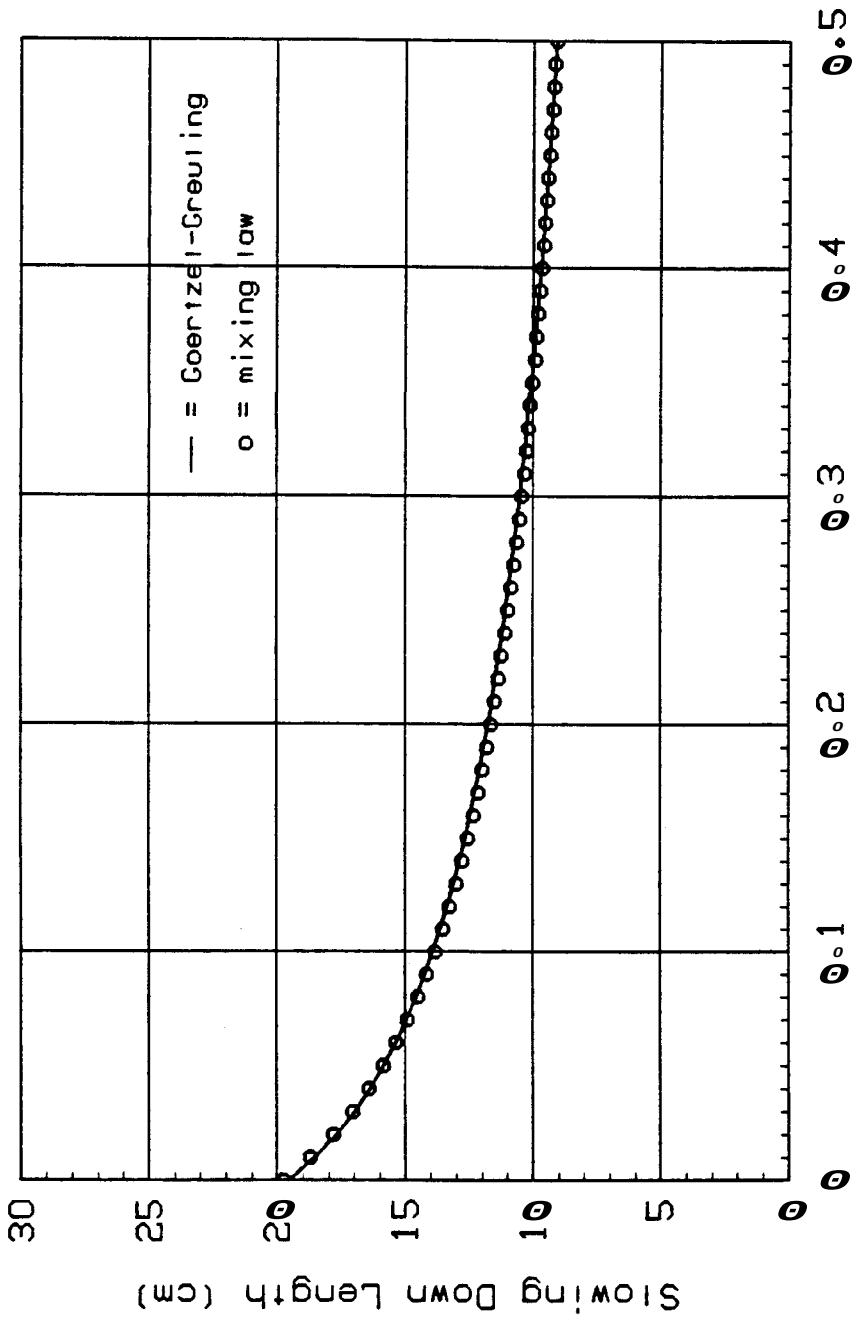

Figure 32. Slowing down length vs. water-filled porosity as predicted by two models indicated for matrix of 90% sandstone, 10% kaolinite.

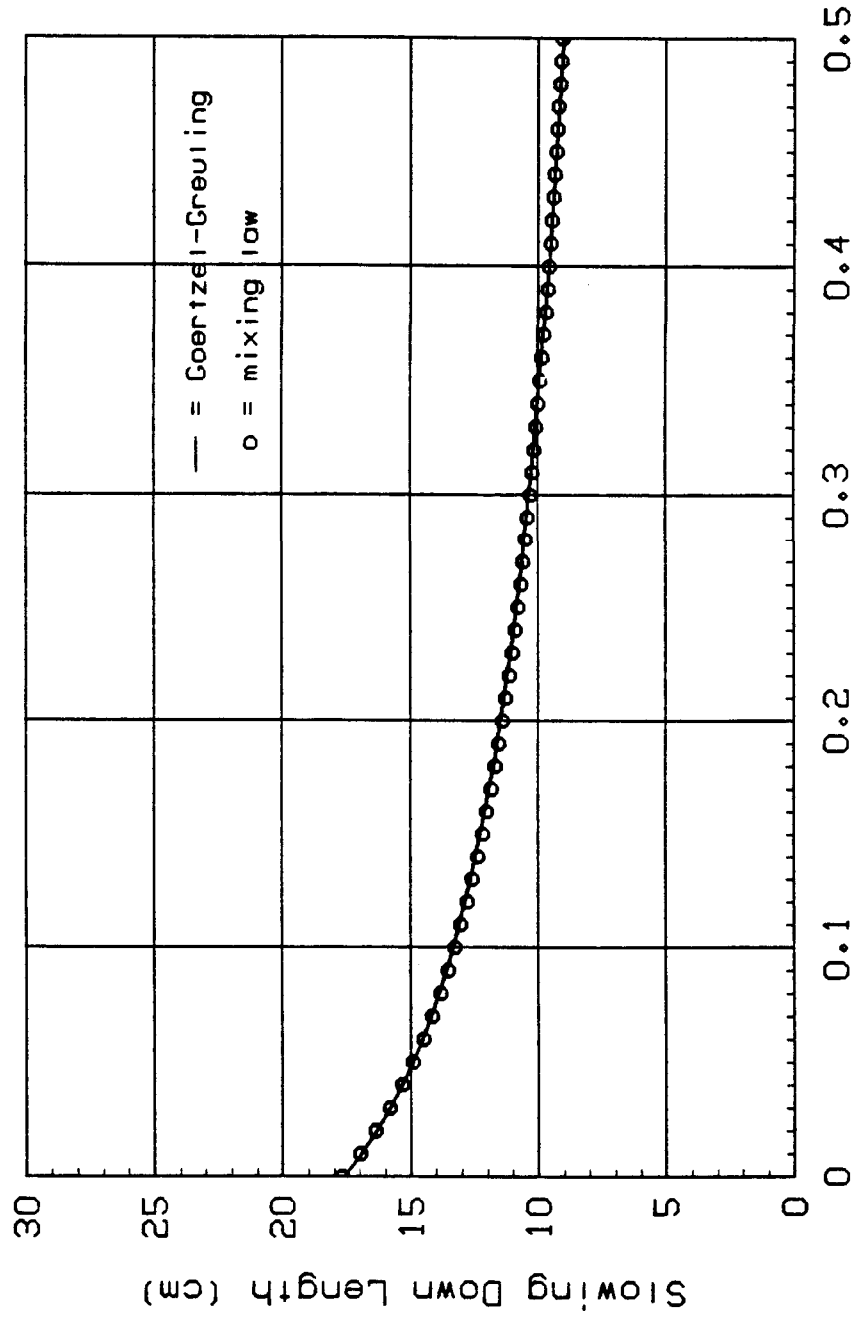

Figure 33. Slowing down length vs. water-filled porosity as predicted by two models indicated for matrix of 85% sandstone, 15% kaolinite

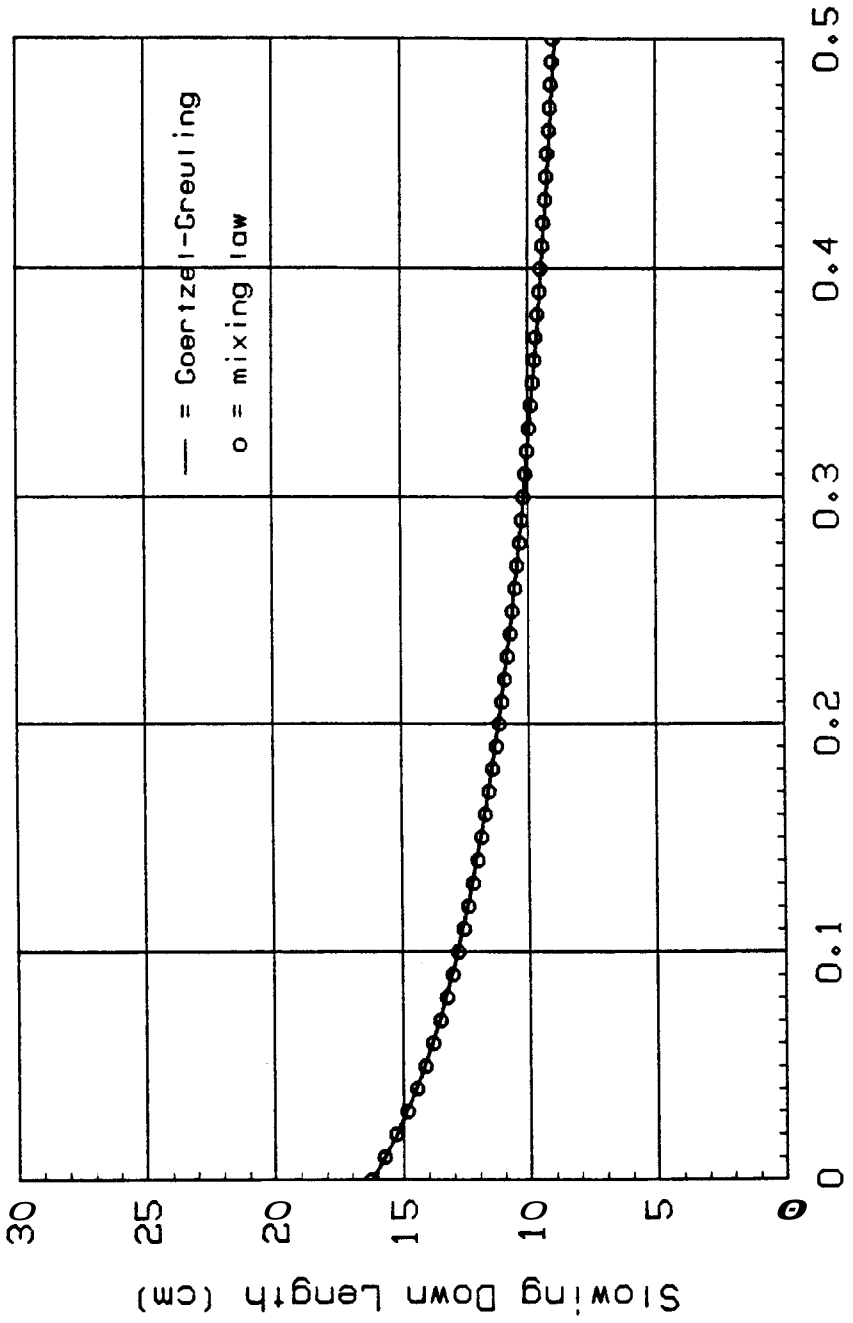

Figure 34. Slowing down length vs. water-filled porosity as predicted by two models indicated for matrix of 80% sandstone, 20% kaolinite.

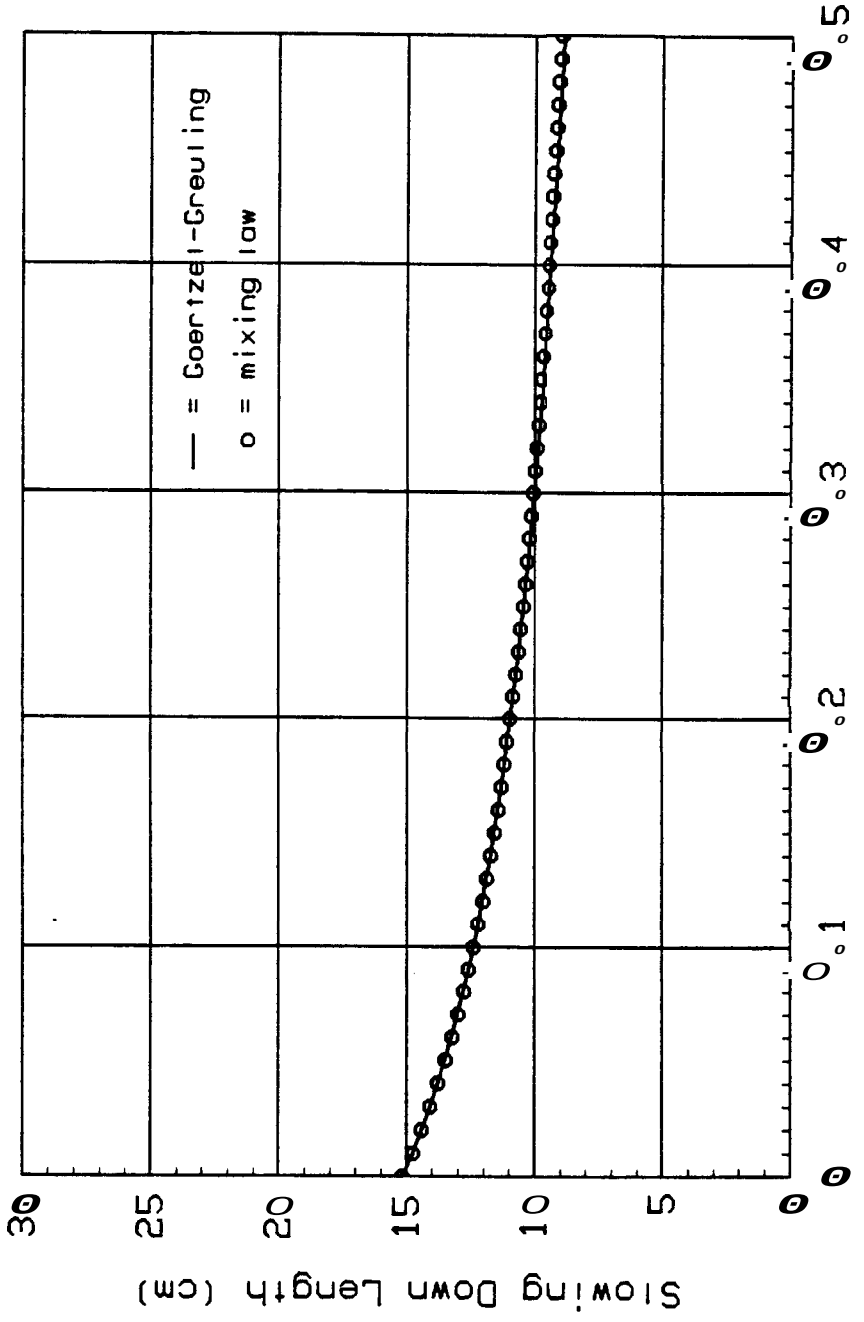

Figure 35. Slowing down length vs. water-filled porosity as predicted by two models indicated for matrix of 75% sandstone, 25% kaolinite.

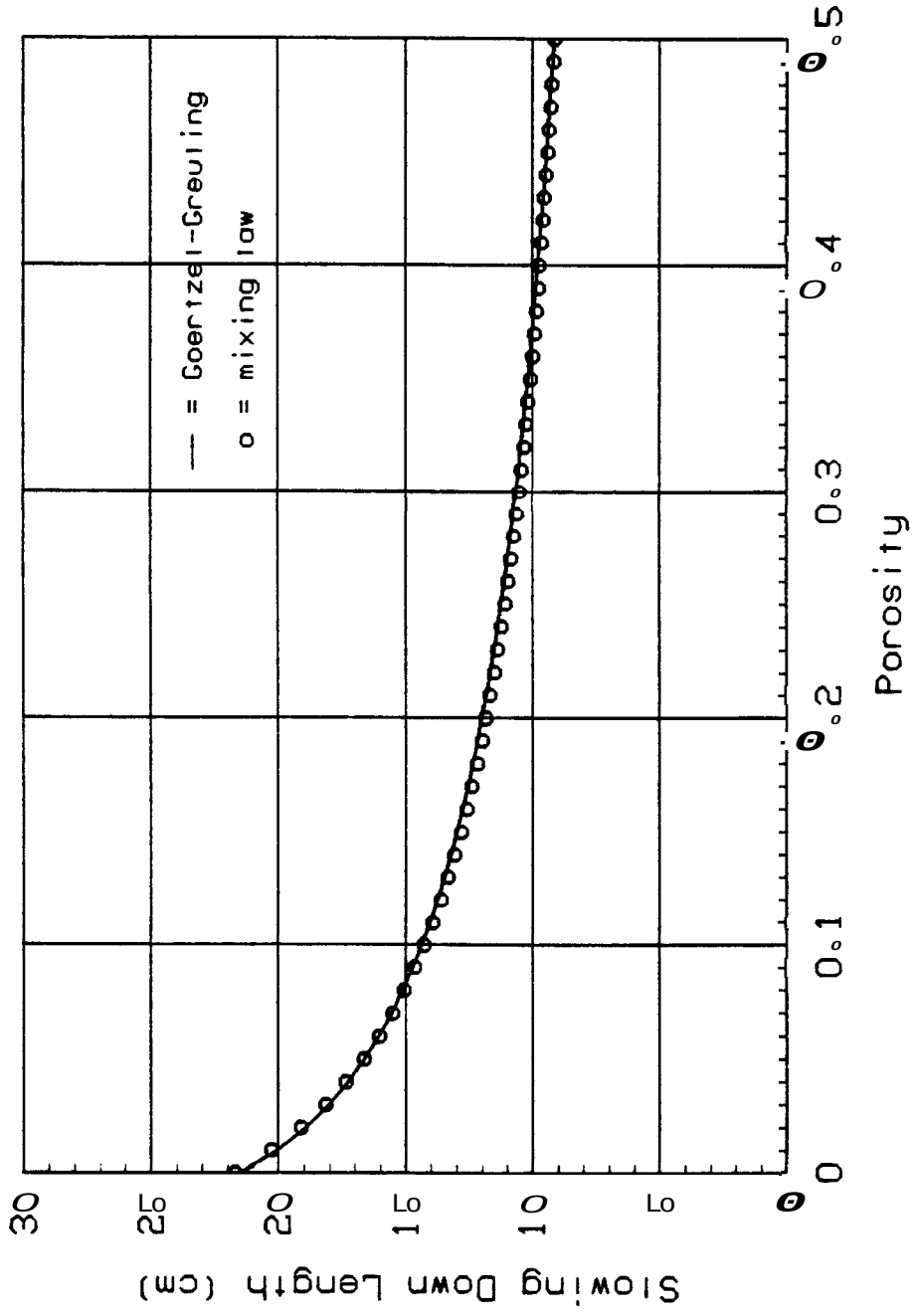

Figure 36. Slowing down length vs. water-filled porosity as predicted by two models indicated for matrix of 90% sandstone, 5% illite, 5% kaolinite.

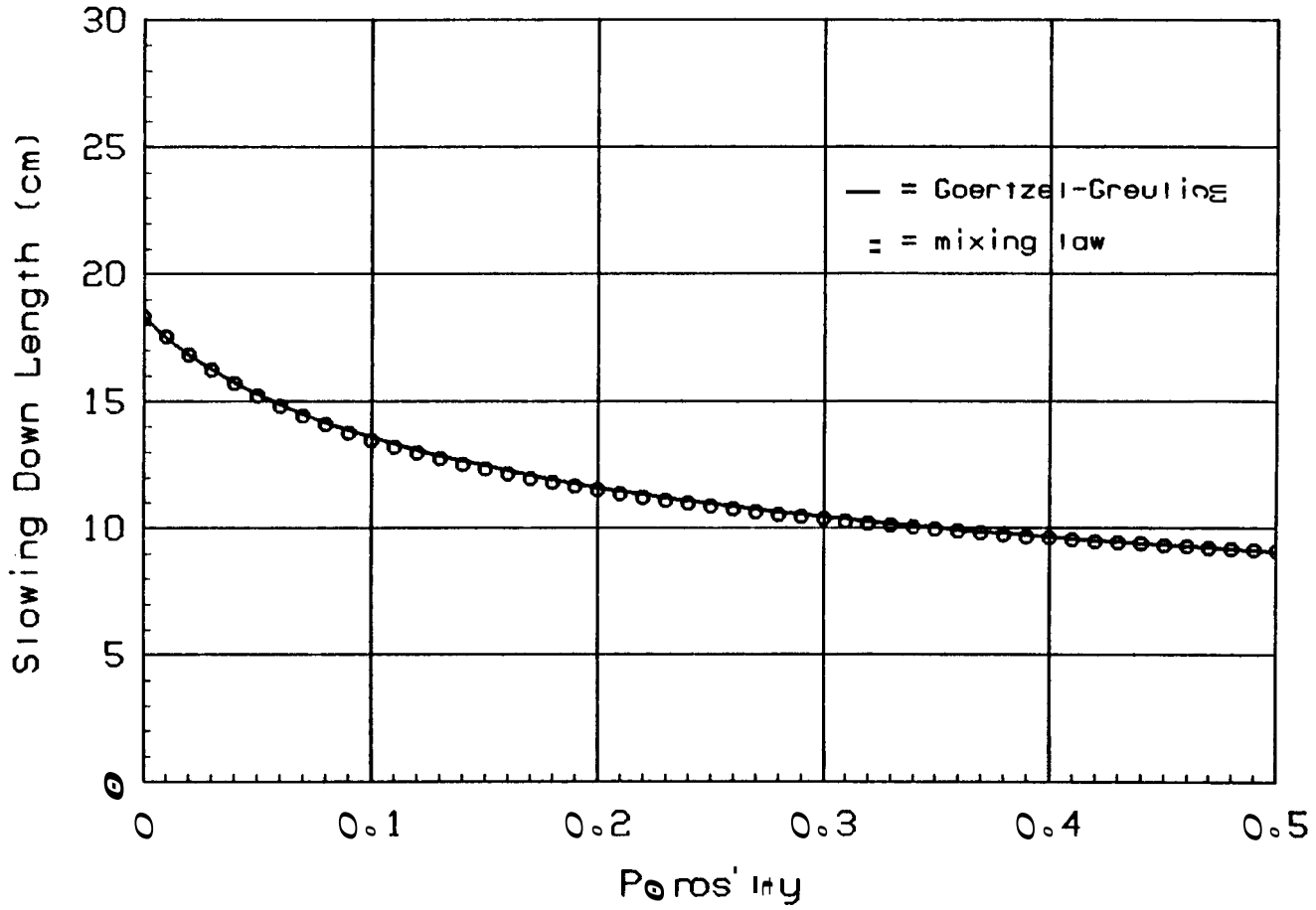

Figure 37. Slowing down length vs. water-filled porosity as predicted by two models indicated for matrix of 80% sandstone, 10% illite, 10% kaolinite.

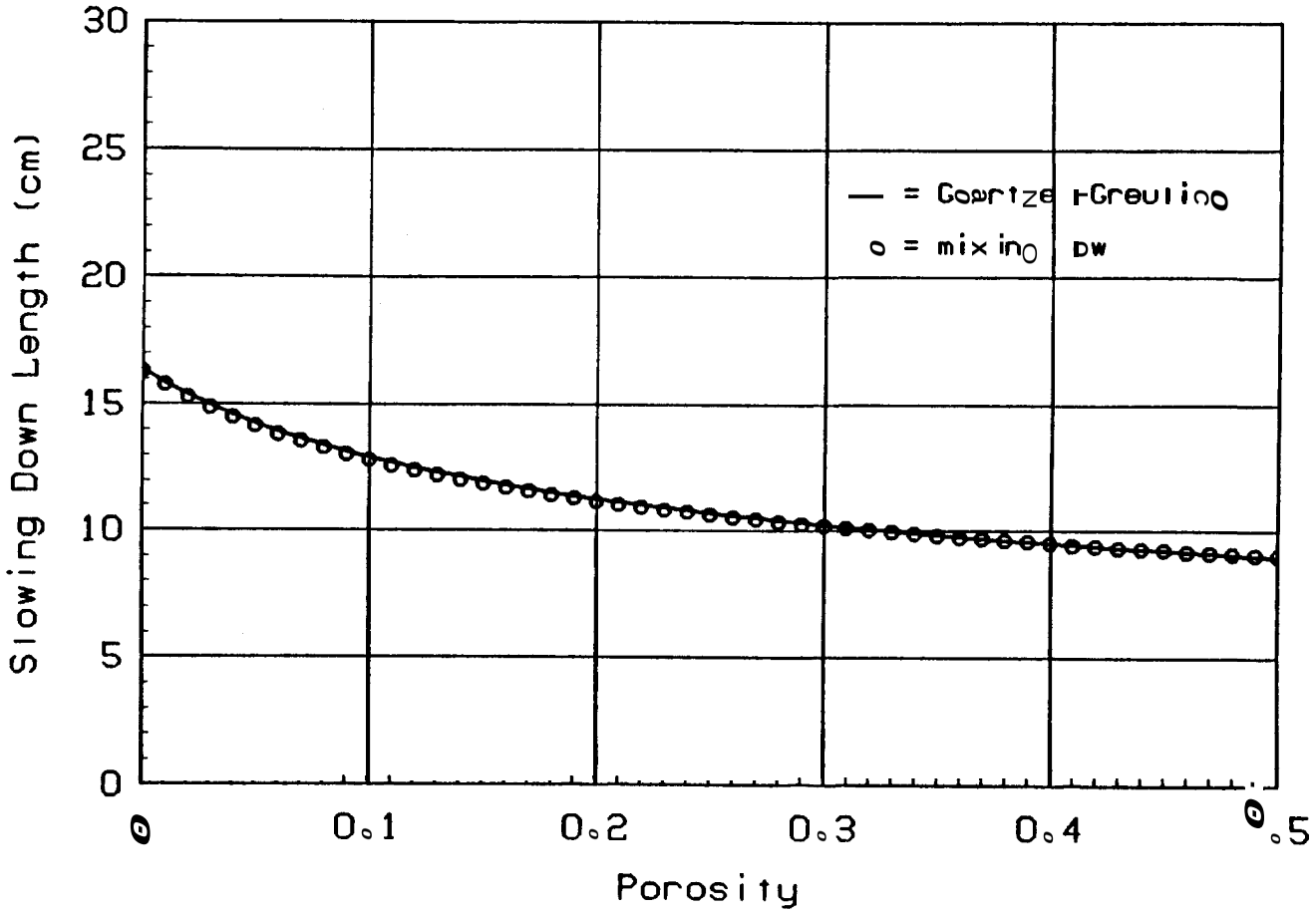

Figure 38. Slowing down length vs. water-filled porosity as predicted by two models indicated for matrix of 70% sandstone, 15% illite, 15% kaolinite.